Mouse models for pancreatic ductal adenocarcinoma are affected by the cre-driver used to promote KRAS^{G12D} activation

Fatemeh Mousavi[1], Joyce Thompson[7], Justine Lau[1], Nur Renollet[7], Mickenzie B. Martin[1], Jake McGue[7], Timothy Frankel[7], Parisa Shooshtari[2,5,6], Christopher L. Pin[1,3-5#], Filip Bednar[7,8#]

Departments of [1]Physiology and Pharmacology, [2]Pathology and Laboratory Medicine, [3]Paediatrics, and [4]Oncology, Schulich School of Medicine and Dentistry, Western University, London, Ontario, Canada; [5]Children's Health Research Institute and Lawson Health Research Institute, London, Ontario, Canada; [6]Ontario Institute for Cancer Research, Toronto, Ontario, Canada; [7]Department of Surgery, University of Michigan, Ann Arbor, Michigan, USA; [8]Program in Cancer Biology, Rogel Cancer Center, University of Michigan, Ann Arbor, Michigan, USA

Correspondence:

Dr. Christopher L. Pin,

A4-917, Cancer Research Laboratory Program

Victoria Campus, London Health Sciences Centre

800 Commissioners Road E

London, ON, N6A 4L6

Telephone: 519-685-8500 x53073

Fax: 519-685-8616

Email: cpin@uwo.ca

Dr. Filip Bednar,

Department of Surgery

2210 Taubman Center

1500 East Medical Center Drive

Ann Arbor, MI 48109

USA

Telephone: 734-936-7607

Email: filipb@med.umich.edu

#Shared senior authorship

Abstract:

The fundamental biology of pancreatic ductal adenocarcinoma has been greatly impacted by the characterization of genetically modified mouse models that allow temporal and spatial activation of oncogenic KRAS ($KRAS^{G12D}$). The most commonly used model involves targeted insertion of a *cre* recombinase into the *Ptf1a* gene. However, this approach disrupts the *Ptf1a* gene, resulting in haploinsufficiency that likely affects sensitivity to oncogenic KRAS ($KRAS^{G12D}$). The goal of this study was to determine if *Ptf1a* haploinsufficiency affected the acinar cell response to $KRAS^{G12D}$ before and after induction of pancreatic injury. We performed morphological and molecular analysis of three mouse lines that express a tamoxifen-inducible *cre* recombinase to activate $KRAS^{G12D}$ in acinar cells of the pancreas. The cre-recombinase was targeted to the acinar-specific transcription factor genes, *Ptf1a* and *Mist1/Bhlha15*, or expressed within a BAC-derived *Elastase* transgene. Up to two months after tamoxifen induction of $KRAS^{G12D}$, morphological changes were negligible. However, induction of pancreatic injury by cerulein resulted in stark differences in tissue morphology between lines within seven days, which were maintained for at least five weeks after injury. $Ptf1a^{creERT}$ pancreata showed widespread PanIN lesions and fibrosis, while the $Mist1^{creERT}$ and *Ela-creERT* models showed reduced amounts of pre-neoplastic lesions. RNA-seq analysis prior to inducing injury suggested $Ptf1a^{creERT}$ and $Mist1^{creERT}$ lines have unique profiles of gene expression that predict a differential response to injury. Multiplex analysis of pancreatic tissue confirmed different inflammatory responses between the lines. These findings suggest understanding the

mechanisms underlying the differential response to *KRAS*^{G12D} will help in further defining the intrinsic KRAS-driven mechanisms of neoplasia initiation.

Key Words: Pancreatic Ductal Adenocarcinoma, Cre Recombinase, KRAS^{G12D}, Ptf1a, Mist1, Elastase, Genetically Engineered Mouse Models

Introduction:

Pancreatic Ductal Adenocarcinoma (PDAC) is the 3rd leading cause of cancer-related deaths in United States. At ~12%, PDAC has the poorest five-year survival rate among the major cancers in United States, which has changed minimally in the past four decades (1). Genetic alterations are found in most PDAC tumours, with >90% of patients harboring somatic mutations in *KRAS*. The most common KRAS mutation causes a glycine to aspartic acid change at amino acid position 12 (*KRAS*^{G12D}), resulting in constitutive activation of KRAS. Oncogenic *KRAS* mutations are observed in pancreatic intraepithelial neoplasias (PanIN) or acinar to duct cell metaplasia (ADM), which are precursor lesions to PDAC (2). However, in vivo studies in mice support a model in which *KRAS*^{G12D} requires additional genetic mutations in tumor suppressors, such as *p53*, *Ink4a*, or *Smad4,* or environmental events, such as pancreatic injury, to progress to PDAC (3).

To understand the cellular and molecular mechanisms that contribute to *KRAS*^{G12D}-mediated PDAC progression, genetically engineered mouse models (GEMMs) have been generated that allow spatial and temporal induction of *KRAS*^{G12D} (4–9). A wide range of GEMMs exist, recapitulating the key features and mutations seen in human

PDAC, including those allowing activation of *KRAS*^{G12D} in combination with the inactivation of *p16*, *p53* or *Smad4*, or with hereditary *Brca1* and *Brca2* mutations (4,10). While initial models focused on generating mutations in key genes during embryonic development, more recent GEMMs have focused on inducible, acinar-specific expression of *KRAS*^{G12D}, which is more representative of the spontaneous mutations seen in patients (11–14). The most commonly used GEMMs involve targeting a tamoxifen-inducible *cre recombinase* to acinar-specific genes, such as *Ptf1a* (*Ptf1a*$^{creERT/+}$*LSL-KRAS*^{G12D}) and *Mist1/Bhlha15* (*Mist1*$^{creERT/+}$*LSL-KRAS*^{G12D}). *Ptf1a* and *Mist1* (*Bhlha15*) are basic helix-loop-helix (bHLH) transcription factors involved in pancreatic development. PTF1A is required for pancreatic formation and specification of acinar cells during pancreatic organogenesis in developing embryos (15,16). Mice homozygous for a null *Ptf1a* mutation survive embryonic development but die shortly after birth (7). *Mist1* is expressed shortly after *Ptf1a* during embryogenesis and promotes acinar cell maturation (17). *Mist1*-null mice are viable but present extensive disorganization of the exocrine pancreas and experience increased tissue damage over time (18,19). *Mist1* has been described as a scaling factor which, rather than initiating transcription of developmental genes, enhances expression of genes required for acinar cell specialization (17,19,20). In the adult pancreas, *Ptf1a* and *Mist1* help maintain the differentiated acinar cell state by regulating expression of genes producing digestive enzymes or regulating exocytosis (15,21,22). Deletion of either transcription factors in adults has been linked to promotion of pancreatic diseases, including PDAC (16,23,24).

Inducible models of PDAC targeting creERT to *Ptf1a* and *Mist1* are functional heterozygotes. However, loss of a single *Ptf1a* gene affects complete acinar cell

differentiation. Ptf1a heterozygotes have enhanced PDAC progression when KRAS^{G12D} is expressed in the developing pancreas (16,25). Whether this difference in sensitivity occurs in the inducible models and affects PDAC progression in adult acini remains an open question. The goal of this study was to compare the effects of KRAS^{G12D} activation in the inducible GEMMs. Morphological and molecular responses to KRAS^{G12D} activation were compared with and without pancreatic injury between mice with a single (*Ptf1a*$^{creERT/+}$*KRAS*$^{G12D/+}$) or two copies (*Mist1*$^{creERT/+}$*KRAS*$^{G12D/+}$ or *Ela-creERT; KRAS*$^{G12D/+}$) of *Ptf1a*. These experiments show a more dramatic response to *KRAS*^{G12D} in *Ptf1a* heterozygotes based on extensive PanIN progression, increased immune infiltration, and an overall phenotype that promotes conditions supportive of KRAS^{G12D}-dependent transformation. These findings confirm *Ptf1a* heterozygosity increases sensitivity to KRAS^{G12D} activation even when limited to adult acinar cells.

Materials and Methods:

Mouse Models

All mice experiments were approved by Animal Care Committee at the University of Western Ontario (2020-157; 2020-158) and the University of Michigan (PRO00009814). Mice at the University of Western Ontario were bred into a C57/Bl6 background and harbored an inducible *loxP-stop-loxP-Kras*^{G12D} (*KRAS*$^{LSL-G12D}$) within the endogenous *Kras* gene. These mice were crossed to mice expressing an inducible cre recombinase (creERT) targeted to either the *Ptf1a* gene (*Ptf1a*$^{creERT/+}$*KRAS*$^{G12D/+}$) or the *Mist1/Bhlha15* gene (*Mist1*$^{creERT/+}$*KRAS*$^{G12D/+}$) to ensure inducible acinar-specific expression of KRAS^{G12D}. These lines resulted in a functional heterozygote for PTF1a or

MIST1 expression. Mice at the University of Michigan were bred into mixed background mice bearing tdTomato (Ela-CreERT) or C57/Bl6 mice bearing YFP (*Ptf1a*$^{creERT/+}$) in the Rosa 26 locus, with and without the *Kras*$^{LSL-G12D}$ allele. The Bac-*Ela-creERT* (*Ela*-creERT) mice contained a BAC-derived transgene with the *Elastase* promoter driving creERT expression (*Ela-creERT; KRAS*$^{G12D/+}$). To induce recombination, 2-4 months old mice were orally gavaged with 3 x 2 (*Mist1*$^{creERT/+}$*KRAS*$^{G12D/+}$) or 5 x 5 mg (*Ptf1a*$^{creERT/+}$*KRAS*$^{G12D/+}$) of tamoxifen (TX; Sigma-Aldrich, T5648-5G) at Western University and 5 x 4 mg (*Ela-creERT; KRAS*$^{G12D/+}$and *Ptf1a*$^{creERT/+}$*KRAS*$^{G12D/+}$) at the University of Michigan over 5 days. This results in >90% recombination for all models (26–28). Mice were either sacrificed 22 days after initial TX gavage or treated with cerulein 1-2 weeks following TX gavage. For cerulein-induced pancreatitis (CIP), mice at Western University received intraperitoneal injections of 50-75 µg/kg cerulein (MedChemExpress, HY-A0190/CS-5876) 8 times over 7 hours, which was repeated after two days. Mice at the University of Michigan received 8 intraperitoneal injections of 75 ug/kg cerulein over 7 hours for two consecutive days. CIP-treated mice were sacrificed 1, 3 or 5 weeks after initial CIP treatment.

Immunohistochemistry (IHC) and Multiplex Immunostaining (Opal):

At the time of sacrifice, pancreata were dissected and prepared for histological, biochemical, or molecular analysis. Pancreatic tissues were fixed in 4% formalin at 4°C overnight, then embedded in paraffin and sectioned to 5 µm. Formalin-fixed paraffin embedded (FFPE) pancreatic tissue sections were deparaffinized and stained for H&E histology or prepared for IHC or immunofluorescence (IF). For IHC, sections were

permeabilized with 0.2% Triton-X in PBS, then blocked for 1 hour in sheep serum with PBS. Following blocking, sections were incubated overnight at 4°C in primary antibodies diluted in blocking solution. Primary antibodies included rabbit α-amylase (1:1000; Abcam, ab21156) and rabbit α-CK19 (1:1000; Abcam, ab52625). Sections were rinsed and incubated for 30 minutes with α-rabbit IgG secondary antibody (1:1000; Vector labs, PK-4001) diluted in blocking solution. For signal detection, the ImmPACT® DAB Substrate Kit (HRP) was used (Vector Laboratories, SK-4105). Images were captured using a Leica Microscope DM5500B DFC365 FX camera with LAS V4.4 software. Positive staining was determined as a percentage of the whole tissue area using ImageJ software.

Alternatively, serial sections (4 µm thick) of FFPE pancreata were stained on the Discovery Ultra XT autostainer (Ventana Medical Systems Inc, Tucson, AZ) for CK19 (1:200) (TROMAIII, University of Iowa hybridoma core) or amylase (1:1500) (A8273, Sigma Aldrich, St Louis, Mo) and counterstained with Mayer's hematoxylin to differentiate between recovered and transformed areas of the pancreas after CIP. Slides were scanned on the Panoramic Scan Digital Slide Scanner (Perkin Elmer) and analyzed for percentage area of positive stain in the QuPath software v0.4.2 (29).

For multiplex analysis, FFPE tissue slides were rehydrated in triplicate with xylene, followed by a single submersion in 100% ethanol, 95% ethanol, and 70% ethanol. Rehydrated slides were washed in neutral buffered formalin and rinsed with deionized water. Antigen retrieval was performed using sodium citrate (pH 6.0) and tris-EDTA (pH

9.0) buffers. Tissue was blocked using endogenous peroxidase at room temperature, followed by 10% donkey serum overnight at 4°C. Primary antibodies for CD3 (1:100, Abcam, Ab11089), CD8 (1:200, Cell Signaling, 98941), F4/80 (1:500, Cell Signaling, 70076), and CK19 (1:400, DSHB, AB 2133570) were diluted in 1% BSA block and sections incubated for 1 hour at RT. After washing with TBST in triplicate, tissues were incubated with secondary antibody, Opal Anti-Ms + Rb HRP (Akoya Biosciences, Marlborough, MA ARH1001EA), before conjugating with Opal fluorophores Following incubation, tissue samples were rinsed in deionized water and mounted with DAPI ProLong™ Diamond Antifade mountant (Thermo Fisher Scientific). Images were taken using the Vectra® Polaris™ work station (Akoya Biosciences).

Multiplex immunofluorescence images were acquired using the Mantra™ Quantitative Pathology work station (Akoya Biosciences). The resulting multispectral slide scan bands (MOTiF) were used for image capture of DAPI, Opal 480 (F4/80), Opal 520 (CD3), Opal 570 (CD8), and Opal 690 (CK19). Slides were scanned and quality of staining assessed after multiplex IHC staining using the Phenochart software (v1.1.0, Akoya Biosciences). The images were then exported for further analysis into QuPath (v0.4.3). For each image, regions of interest of 1 mm2 were tiled over the tissue to cover >90% of the tissue and exclude peripancreatic fat and any peripancreatic or intraparenchymal lymph nodes. Initial cell detection in each image was done using in the DAPI channel (settings – pixel size 0.5mm, background radius 8mm, median filter 0mm, sigma 1.5mm, minimal area 10mm2, maximum area 400mm2, threshold 10, split by shape – YES, cell expansion 3mm, cell nucleus included). Spot check of 10% of

ROIs in each images confirmed consistent selection of all cells in all regions. Annotation of identified cells was then performed using either a threshold classifier approach using the cell/cytoplasm maximum marker fluorescence (CD3, CD8, CK19) or the random decision tree machine learning approach within QuPath (F4/80). The classifier leveraged the significantly different morphology of myeloid cells and pancreatic acinar cells and was trained using both fluorescence and morphologic cell characteristics for the classification. Manual spotcheck of all classifiers across multiple ROI in all images revealed <5% of incorrect cell classification using these approaches. The primary issue arose due to compact packing of cells in some areas of the tissue, where fluorescent bleedthrough from a cell affected phenotype classification of its neighbor yielding incompatible phenotypes such as CD3+/F4/80+ cells or CD3+/CK19+ cells. These cases were rare and after manual curation, appropriate phenotypes were able to be assigned in vast majority of these cells. The final phenotype quantification of all cells in each ROI for each image was exported into text data files. Final statistical analysis and data visualization was performed in R (v 4.2.1, packages – tidyverse 1.3.2, pheatmap 1.0.12, RColorBrewer 1.1-3, viridis 0.6.2). Statistical analysis was done with a Kruskal-Wallis rank sum test and subsequent pairwise Wilcoxon rank sum test with $p<0.05$ considered to be significant.

RNA isolation, RNA-seq and data analysis

RNA was isolated from pancreatic tissue 22 days after initial TX gavage using Trizol (ThermoFisher Scientific, 15596018) and the PureLink RNA mini kit (ThermoFisher Scientific, 12183018A). RNA quality was confirmed using an Agilent 2100 Bioanalyzer

and sequenced to a depth of 50 million reads/sample using the Illumina NextSeq High Output 150 cycle (paired-end sequencing) sequencing kit. For RNA-seq analysis, sequence quality was assessed using FastQC, reads were mapped to the mm10 genome using STAR 2.7.9a (30), counted using the featureCounts option in the Subread aligner v2.0.3 (31), and analyzed for differential expression using DESeq2 package v1.38.3 (32) in RStudio. Batch effect correction and data normalization was performed through built-in DESeq2 features. KEGG and GO pathway analyses were performed using clusterProfiler v4.6.2 R package (33), Gene Set Enrichment Analysis (GSEA) was done using fgsea v1.24.0 R package (34), and heatmaps generated using pheatmap v1.0.12 R package (35). PCAtools 2.10.0 (36) and enrichplot v1.18.4 (37) were used for generating PCA plots and dotplots. Gene sets used for enrichment analysis and visualization were obtained from MSigDB (38,39) and Harmonizome (40). Differentially expression gene (DEG) were defined as any gene with a p-value < 0.05 and fold change (FC) > 2. A threshold of adjusted p-value $\leqq 0.05$ was set for all pathway analyses.

Results:

Previous studies suggested loss of a single *Ptf1a* allele alters the molecular landscape of acinar cells (16). To determine if this affects the response to oncogenic KRAS ($KRAS^{G12D}$) in adult acinar cells, we compared the morphology of pancreatic tissue 22 days after induction of $KRAS^{G12D}$ in 2 to 4-month-old mice in which creERT was targeted to either the *Ptf1a* or *Mist1* gene (Figure 1A, B), which renders the single floxed allele non-functional. $Ptf1a^{creERT/+}KRAS^{G12D/+}$ and $Mist1^{creERT/+}KRAS^{G12D/+}$ pancreata

showed normal pancreatic morphology with no pre-neoplastic lesions. Therefore, we initiated CIP 10 days after the last tamoxifen (TX) treatment to promote pancreatic injury (Figure 1C). Mice received two days of cerulein compared, and compared morphology was compared five weeks after initial cerulein treatment. H&E histology of *Ptf1a*$^{creERT/+}$*KRAS*$^{G12D/+}$ mice revealed an almost complete loss of acinar tissue with extensive regions of low (PanIN2) or high (PanIN3) grade lesions, consistent with our previous work (27). Conversely, significantly fewer PanIN lesions and more acinar tissue was observed in *Mist1*$^{CreERT/+}$*KRAS*$^{G12D/+}$ mice ($p < 0.0005$, Figure 1D, E). To confirm the differential maintenance of acinar tissue, IHC for markers of acinar (amylase) and duct (CK19) cells was performed. *Ptf1a*$^{creERT/+}$*KRAS*$^{G12D/+}$ pancreata showed significantly more CK19 staining (21.66 ± 3.12%) than *Mist1*$^{creERT/+}$*KRAS*$^{G12D/+}$ tissue (3.94 ± 3.12%, $p < 0.005$), and minimal amylase staining (0.65 ± 12.89%, $p < 0.05$) compared to *Mist1*$^{creERT/+}$*KRAS*$^{G12D/+}$ tissue (66.52 ± 12.89%), confirming increased transformation occurred in the *Ptf1a*$^{creERT/+}$*KRAS*$^{G12D/+}$ mice (Figure 1F-H).

To determine if the loss of a single *Ptf1a* allele was the cause of a different response to KRAS^{G12D}, *Ptf1a*$^{creERT/+}$*KRAS*$^{G12D/+}$ mice bred in a different institute were compared to a second mouse model that retains two copies of the *Ptf1a* gene. In these mice, KRAS^{G12D} is induced in a transgenic mouse model in which creERT is expressed under the control of the *Elastase* promoter within a bacterial artificial chromosome construct (BAC). In the absence of cerulein, neither mouse line showed pre-neoplastic lesions, similar to earlier findings (Figure 2A). Once again, initiation of CIP in these mice 7 days after induction of *KRAS*^{G12D} resulted in widespread PanINs in *Ptf1a*$^{creERT/+}$*KRAS*$^{G12D/+}$

mice extending through the entire tissue (Figure 2B, C). Similar to the *Mist1*$^{creERT/+}$*KRAS*$^{G12D/+}$ mice, *Ela-creERT; KRAS*$^{G12D/+}$ tissue showed less CK19 IHC staining indicative of fewer PanINs (1.42 ± 0.606%) relative to *Ptf1a*$^{creERT/+}$*KRAS*$^{G12D/+}$ tissue (15.9 ± 1.22, $p < 0.0001$) and retained more acinar cell tissue (62.0 ± 4.97%) compared to the *Ptf1a*$^{creERT/+}$*KRAS*$^{G12D/+}$ tissue (33.5 ± 5.38%, $p < 0.0041$) as indicated by amylase IHC staining (Figure 2D-F). These findings support a model in which absence of a single *Ptf1a* allele increases the sensitivity to KRAS^{G12D}-mediated PanIN progression.

To determine if the increased transformation observed in *Ptf1a* heterozygous mice was due to a differential response to injury (i.e. the acinar cells had differential sensitivity) or a differential ability to recover (i.e. the resulting ADM lesions had differential sensitivity), pancreatic morphology was examined 7 days after the initial CIP treatment in all lines (Figure 3). Consistent with longer time points, *Ptf1a*$^{creERT/+}$*KRAS*$^{G12D/+}$ mice showed extensive loss of acinar tissue with widespread PanIN lesion formation (Figure 3B, D), while *Mist1*$^{creERT/+}$*KRAS*$^{G12D/+}$ (Figure 3B) and *Ela*^{creERT}*KRAS*$^{G12D/+}$ mice (Figure 3D) retained higher amounts of acinar tissue suggesting loss of a single *Ptf1a* allele increases sensitivity to KRAS^{G12D} and is not simply preventing regeneration.

Next, to determine the mechanisms underlying this differential response to KRAS^{G12D} between *Ptf1*$^{+/-}$ and *Ptf1*$^{+/+}$ tissue, RNA-seq was performed 22 days after initial TX treatment on pancreatic tissue obtained from *Ptf1a*$^{creERT/+}$*KRAS*$^{G12D/+}$ and *Mist1*$^{creERT/+}$*KRAS*$^{G12D/+}$ mice in the absence of pancreatic injury (Figure 4). This

experimental timeline was chosen since no morphological differences were observed between *Ptf1a*$^{creERT/+}$*KRAS*$^{G12D/+}$ and *Mist1*$^{creERT/+}$*KRAS*$^{G12D/+}$ pancreatic tissue (Figure 1B). Principal Component Analysis (PCA) comparing *KRAS*^{G12D}-expressing and WT pancreata of each line showed distinct clustering of the groups based on their genotype (4A, B), suggesting underlying differences at the transcriptomic level even in the absence of any observable histologic difference. Surprisingly, *Mist1*$^{creERT/+}$*KRAS*$^{G12D/+}$ mice have more differentially expressed genes (DEGs) compared to wild type mice (Figure 4C; 784 DEGs, 439 up and 345 down) than *Ptf1a*$^{creERT/+}$*KRAS*$^{G12D/+}$ mice compared to wild type mice (Figure 4D; 461 DEGs, 374 up and 87 down). A higher percentage of the DEGs in the *Ptf1a*$^{creERT/+}$*KRAS*$^{G12D/+}$- wild type dataset was upregulated indicating involvement of active regulatory processes.

Next, Gene Set Enrichment Analysis (GSEA) was performed using MSigDB's hallmark gene sets comparing *Ptf1a*$^{creERT/+}$*KRAS*$^{G12D/+}$ and *Mist1*$^{creERT/+}$*KRAS*$^{G12D/+}$ to their respective wild type control tissues. Multiple cancer-related gene sets were differentially enriched between lines (Figure 4E), including positive enrichment of genes defining epithelial-mesenchymal transition, Kras signaling, and inflammatory response. These differences appeared in the absence of morphological changes in pancreatic tissue suggesting unique molecular gene expression profiles exist between the lines prior to phenotypic transformation.

One of the gene sets identified by GSEA was genes up-regulated by KRAS activation (HALLMARK_KRAS_SIGNALING_UP). This pathway was positively enriched

compared to wild type tissue in the presence of one *Ptf1a* allele (*Ptf1a*$^{creERT/+}$*KRAS*$^{G12D/+}$) but negatively enriched when two *Ptf1a* alleles were present (*Mist1*$^{creERT/+}$*KRAS*$^{G12D/+}$; Figure 5A). Comparison of normalized *KRAS* read counts from the sequencing files indicates an increase in expression, but these increases were not significant in either the *Ptf1a*$^{creERT/+}$*KRAS*$^{G12D/+}$ - wild type or *Mist1*$^{creERT/+}$*KRAS*$^{G12D/+}$ - wild type comparisons (Figure 5B), and *Kras* was not identified as a DEG in either dataset. This suggests the positive enrichment for KRAS signaling in the *Ptf1a*$^{creERT/+}$*KRAS*$^{G12D/+}$ pancreas is due to upregulation of downstream KRAS effectors rather than differences in *KRAS* expression. Plotting normalized read counts of genes in the MAPK signaling pathway from the KEGG pathways dataset for wild type and *Ptf1a*$^{creERT/+}$*KRAS*$^{G12D/+}$ RNA shows an overall pattern of increased expression for the MAPK pathway in *Ptf1a*$^{creERT/+}$*KRAS*$^{G12D/+}$ mice (Figure 5C). In confirmation of this, IHC for FOS, a member of the Activator Protein 1 (AP-1) transcriptional complex, downstream mediator of KRAS signaling in the MAPK pathway, and identified as a DEG only in *Ptf1a*$^{creERT/+}$*KRAS*$^{G12D/+}$ mice, showed increased accumulation in the *Ptf1a*$^{creERT/+}$*KRAS*$^{G12D/+}$ pancreas compared to *Mist1*$^{creERT/+}$*KRAS*$^{G12D/+}$ tissue, but only after induction pancreatic injury (Figure 5D). JUN, a binding partner for FOS did not show the same increased expression in IHC. This is in line with the RNA-seq data as *Jun*, unlike *Fos*, does not show differential expression of Jun at the transcriptomic level (Figure 5E). Combined, these findings suggest the loss of a single *Ptf1a* allele causes differential enrichment of KRAS signaling, which may account for the more aggressive phenotypes in pancreatic cancer mouse models.

Next, the molecular profile of the two lines were assessed by Gene Ontology (GO) pathway analysis. 154 GO pathways were enriched based on the *Mist1*$^{creERT/+}$*KRAS*$^{G12D/+}$ - wild type comparison set, while 403 pathways were enriched based on the *Ptf1a*$^{creERT/+}$*KRAS*$^{G12D/+}$ - wild type comparison set. However, only 15 pathways were common between these two comparisons. The top pathways uniquely enriched in the *Ptf1a*$^{creERT/+}$*KRAS*$^{G12D/+}$ - wild type comparison set were almost exclusively immune-related (Figure 6A, B), similar to the GSEA findings which indicated hallmark genes in the Inflammatory Response gene set are differentially enriched between *Ptf1a*$^{creERT/+}$*KRAS*$^{G12D/+}$ and *Mist1*$^{creERT/+}$*KRAS*$^{G12D/+}$ tissues (Figure 4E). GSEA shows significantly positive enrichment in the *Ptf1a*$^{creERT/+}$*KRAS*$^{G12D/+}$ - wild type comparison set (NES= 2.4; Figure 6c) and significant negative enrichment *Mist1*$^{creERT/+}$*KRAS*$^{G12D/+}$ - wild type comparison set (NES= -1.9). These results predict a differential inflammatory response between *Ptf1a*$^{creERT/+}$*KRAS*$^{G12D/+}$ and *Mist1*$^{creERT+}$*KRAS*$^{G12D/+}$ mice.

To examine immune cell infiltration following CIP in the two mouse lines, we performed an Opal Multiplex assay for multiple immune marks in *Ptf1a*$^{creERT/+}$*KRAS*$^{G12D/+}$ and *Mist1*$^{creERT+}$*KRAS*$^{G12D/+}$ mice one week after CIP (Figure 7). CK19 IF showed reduced staining in *Mist1*$^{creERT+}$*KRAS*$^{G12D/+}$ tissue compared to *Ptf1a*$^{creERT/+}$*KRAS*$^{G12D/+}$ (Figure 7A, B) consistent with earlier analysis. F4/80 accumulation marks macrophages and is generally correlated with the level of CK19 staining observed in the tissue. *Ptf1a*$^{creERT/+}$*KRAS*$^{G12D/+}$ pancreata showed the highest load of macrophage infiltration around lesions (average percent per tile= 25.8%; Figure 7A, C). CD8+ T cells (average

percent per tile= 0.18%; Figure 7A, D) were significantly lower in number compared to macrophages, but still showed significantly more accumulation in *Ptf1a*$^{creERT/+}$*KRAS*$^{G12D/+}$ tissue compared to *Mist1*$^{creERT+}$*KRAS*$^{G12D/+}$ tissue. CD3^{+} T cells (average percent per tile= 0.04%; Figure 7A, E) did not show any significant difference between the two lines. Hierarchical clustering of the expression level of each immune marker in *Ptf1a*$^{creERT/+}$*KRAS*$^{G12D/+}$, *Mist1*$^{creERT+}$*KRAS*$^{G12D/+}$, and wild type tissues following quantification confirmed a higher percentage of lesions (CK19) and macrophage infiltration (F4/80) in the *Ptf1a*$^{creERT/+}$*KRAS*$^{G12D/+}$ tissue (Figure 7F) suggesting a correlation between CK19 and F4/80 staining (Figure 7G) consistent with the observed macrophage infiltration around CK19+ ADM and PanINs.

To determine if the differential immune cell infiltration also occurs between the *Ptf1a*$^{creERT/+}$*KRAS*$^{G12D/+}$ and *Ela-creERT; KRAS*$^{G12D/+}$ mouse lines, similar analysis was performed 1 week following CIP (Figure 8). Surprisingly, *Ptf1a*$^{creERT/+}$*KRAS*$^{G12D/+}$ tissue did not show increased CK19+ lesions compared to *Ela-creERT; KRAS*$^{G12D/+}$ tissue (Figure 8A, B) even though the number of progressed lesions are more in *Ptf1a*$^{creERT/+}$*KRAS*$^{G12D/+}$. However, Opal Multiplex assays for F4/80 showed *Ptf1a*$^{creERT/+}$*KRAS*$^{G12D/+}$ pancreata had increased macrophage infiltration (Figure A, C) compared to *Ela-creERT; KRAS*$^{G12D/+}$ tissue with no difference observed between the two lines for CD8^{+} and CD3^{+} T cell infiltration (Figure 8A, D, E). Hierarchical clustering of the expression level of each immune marker in *Ptf1a*$^{creERT/+}$*KRAS*$^{G12D/+}$, *Ela-creERT; KRAS*$^{G12D/+}$, and the wild type tissues following quantification confirmed a higher percentage of F4/80 staining (Figure 8F). The higher level of CK19 staining in the *Ela-*

creERT; KRAS$^{G12D/+}$ tissue does not seem to be correlated with higher level of macrophage infiltration (Figure 8G), which could suggest that the higher percentage of CK19 positive cells in these mice are a byproduct of normal ducts and recovering stressed acinar cells with residual CK19 signal. There is however a positive correlation between CK19 staining and macrophage infiltration in the *Ptf1a*$^{creERT/+}$*KRAS*$^{G12D/+}$ tissue (Figure 8G). These findings support a model in which immune-related pathways are differentially activated in *Ptf1a*$^{creERT/+}$*KRAS*$^{G12D/+}$ mice. These observations confirm RNA-seq analysis showing differential enrichment of immune-related pathways between lines and that loss of a single *Ptf1a* alleles may prime the tissue for a differential immune response even before appearance of any lesions.

Discussion:

Pancreatic ductal adenocarcinoma has the highest mortality rate of the major cancers, with few effective therapeutic options available. Significant advances have been made on the fundamental mechanisms in PDAC initiation and progression through the development of GEMMs. Since the development of the KC mice (41), the first conditional mouse model resulting from breeding *Pdx1-cre* or *Ptf1a-cre* mice to *KRAS*$^{LSL-G12D}$ mice, additional genetic mouse models of PDAC have been developed, including inducible and non-inducible models, each informing a unique aspect of PDAC. All these models use an oncogenic KRAS mutation (*KRAS*^{G12D} or *KRAS*^{G12V}) with the goal of generating temporal and/or spatial activation to mimic the etiology of human PDAC more accurately. Differences have been noted between inducible and non-inducible models of PDAC, and there are indications different cre recombinase drivers may have unique phenotypes. However, to date, a direct comparison between lines has

not been published. In this study we characterized the molecular and phenotypic differences between *Ptf1a*$^{creERT/+}$*KRAS*$^{G12D/+}$, *Mist1*$^{creERT/+}$*KRAS*$^{G12D/+}$, and *Ela-creERT; KRAS*$^{G12D/+}$ mouse lines as these models are among the most used tamoxifen-inducible models allowing Kras expression in adult acinar cells. Our results show clear differences in the molecular response to *KRAS*^{G12D} that correlates to marked differences between the lines and highlights the importance for choosing the right model for studying different aspects of pancreatic cancer.

Pancreatic Transcription Factor 1a (PTF1a) is a regulator of pancreatic organogenesis, essential for pancreatic determination, exocrine fate decision, acinar cell differentiation, and activation of other key transcription factors (15,42–44). Null mutations in *Ptf1a* lead to absence of exocrine pancreas and is lethal in mice (7). Our results suggest *Ptf1a* haploinsufficiency resulting from targeted insertion of cre recombinase correlated to increased sensitivity to *KRAS*^{G12D} indicated by increased PanIN progression and loss of the mature acinar cell phenotype. These findings are consistent with studies suggesting *Ptf1a*'s function is dosage-dependent, with reduced expression leading to pancreatic hypoplasia, diminished expression of exocrine genes, and ultimately maintenance of progenitor fate (45–47). Furthermore, adult acinar cells in *Ptf1a* heterozygous mice proliferate more than the corresponding wild type mice (48) and *Pdx1*^{cre}*KRAS*^{G12D} mice harboring a heterozygous deletion of *Ptf1a* show increased PanINs compared to *Ptf1a* wild type counterparts (16). Our RNA-seq results support a dosage-dependent function of *Ptf1a* and show loss of a single allele is sufficient to alter the molecular response to KRAS^{G12D}, even in the absence of morphological changes to the pancreas (Figure 4).

Our data suggests loss of one *Ptf1a* allele correlates to increased KRAS signaling, which may account for the increased PDAC progression compared to those lines that retain both copies of *Ptf1a*. This is supported by findings in other studies demonstrating loss of *Ptf1a* gene activates KRAS-dependency and that *Ptf1a* prevents KRAS-driven PDAC progression (16,49).

RNA-seq also suggested an enrichment of inflammatory and immune-related pathways in *Ptf1a*$^{creERT/+}$*KRAS*^{G12D} mice compared to *Mist1*$^{creERT/+}$*KRAS*^{G12D} mice even before the induction of injury. Significantly increased accumulations of macrophages in *Ptf1a*$^{creERT/+}$*KRAS*^{G12D} pancreas, particularly around lesion areas, were observed compared to wild type or *Mist1*$^{creERT/+}$*KRAS*^{G12D} pancreas. This finding reinforces a model in which solid tumors, including PDAC tumor cells, trigger inflammation that recruits immunosuppressive leukocytes, such as macrophages, to the lesion site (50,51). This increased infiltration is a response to KRAS^{G12D} that is programmed early in the initiation stages of the disease, as we see a differential transcriptomic profile before appearance of any lesions that supports myeloid cell differentiation and migration in the *Ptf1a*$^{creERT/+}$*KRAS*^{G12D} mice. This observation is supported by findings from Zhang et al. study indicating that depletion of myeloid cells early during PDAC development prevents PanIN progression (52). The same study showed myeloid cells to be required for sustained MAPK signaling during carcinogenesis, which ultimately promotes immune evasion through a mechanism involving EGFR/MAPK-dependent regulation of PD-L1 expression (52). Similarly in our experiment, along with enrichment of myeloid cell-related pathways and increased F4/80 staining, there is a distinct increase in MAPK

pathway-related genes (Figure 5) with the loss of a *Ptf1a* allele (*Ptf1a*$^{creERT/+}$*KRAS*^{G12D}) that was not seen when both *Ptf1a* alleles were functional (*Mist1*$^{creERT/+}$*KRAS*^{G12D} and *Ela-creERT; KRAS*$^{G12D/+}$). This finding proposes a multilateral role for dose-dependency of *Ptf1a* in PDAC progression, understanding which not only contributes to enhancing mouse models studying this progression but may also provide a novel therapeutic strategy for PDAC.

While macrophages represent the most dominant immune cells present in the microenvironment in our study, CD3^{+} and CD8^{+} T-cells showing far less accumulation around PanIN lesions. Macrophage recruitment excludes T-cells from the microenvironment (53), as evident by the scarce number of effector T cells in pre-invasive and invasive PDAC (51). While the overall number of CD8+ and CD3+ T-cells in our study is low in both *Ptf1a*$^{creERT/+}$*KRAS*^{G12D} and *Mist1*$^{creERT/+}$*KRAS*^{G12D} pancreata, the number of CD8+ T cells is significant higher in *Ptf1a*$^{creERT/+}$*KRAS*^{G12D} pancreas compared to *Mist1*$^{creERT/+}$*KRAS*^{G12D}. The heightened aggressivity of the *Ptf1a*$^{CreERT/+}$ response to *KRAS*^{G12D} may cause a more pronounced immune response in these mice. Whether these T-cells show optimal activation and function and whether they maintain their increased numbers compared to the *Mist1*$^{creERT/+}$*KRAS*^{G12D} mice as the disease progresses should be addressed in future studies.

Overall, our results show that even without pancreatic injury or morphological differences, KRAS^{G12D} promoted unique transcriptomic profiles based on PTF1A dosage, including differential activation of KRAS signaling and enrichment of immune-

related pathways. The more extensive lesions and increased immune infiltration suggest *Ptf1a* haploinsufficient mice are primed by $KRAS^{G12D}$, possibly through epigenetic reprogramming, for a differential downstream cascade of events following a second environmental stimulus such as inflammation. Epigenetically primed genes are poised to rapidly respond to external cues, a process utilized during development to regulate cellular differentiation and plasticity (54–58), and observed in a number of diseases including neurodevelopmental disorders, immunodeficiencies, and cancers (59–61). Epigenetic reprogramming of poised genes can increase the sensitivity of pancreatic cells undergoing stress to chronic pancreatitis (62), a risk-factor for PDAC. Future studies are necessary to elucidate whether a link between *Ptf1a* haploinsufficiency and epigenetic mechanisms underlie the differential response to $KRAS^{G12D}$ activation.

In summary, this study highlights the effect of *Ptf1a* haploinsufficiency and dose-dependency on the response to $KRAS^{G12D}$ activation in adult acinar cells. Our findings suggest loss of a single *Ptf1a* allele alters the response to $KRAS^{G12D}$ activation in adult acinar cells, leading to more aggressive phenotypes. One underlying mechanism for this altered response appears to involve differentially priming of genes that include, amongst other things, pathways involved in potentiating KRAS signaling and a pro-inflammatory response at early stages even before the appearance of pre-neoplastic lesions. Follow-up studies investigating such epigenetic mechanisms are necessary to further elucidate the effects of *Ptf1a* haploinsufficiency on PDAC progression and the prognostic significance of lower expression levels of *Ptf1a* in PDAC patients.

Acknowledgements and Funding:

The authors wish to acknowledge the ongoing support of several national research funding agencies for this work including the Canadian Institutes of Health Research (MOP#PJT166029), the Cancer Research Society of Canada and the Rob Lutterman Foundation for Pancreatic Cancer Research. This work would not be possible without specific support from a London Regional Cancer Centre Catalyst Grant, co-supported by Mr. Keith Sammit and an internal bridge grant from the University of Western Ontario. FM is supported by Mitacs Accelerate Fellowship.

References:

1. Siegel RL, Miller KD, Wagle NS, Jemal A. Cancer statistics, 2023. CA Cancer J Clin [Internet]. 2023 Jan 12;73(1):17–48. Available from: https://onlinelibrary.wiley.com/doi/10.3322/caac.21763
2. Hu H feng, Ye Z, Qin Y, Xu X wu, Yu X jun, Zhuo Q feng, et al. Mutations in key driver genes of pancreatic cancer: molecularly targeted therapies and other clinical implications. Acta Pharmacol Sin [Internet]. 2021 Nov 11;42(11):1725–41. Available from: https://www.nature.com/articles/s41401-020-00584-2
3. Guerra C, Schuhmacher AJ, Cañamero M, Grippo PJ, Verdaguer L, Pérez-Gallego L, et al. Chronic Pancreatitis Is Essential for Induction of Pancreatic Ductal Adenocarcinoma by K-Ras Oncogenes in Adult Mice. Cancer Cell. 2007 Mar;11(3):291–302.
4. Leach SD. Mouse models of pancreatic cancer. Cancer Cell. 2004 Jan;5(1):7–11.
5. Apelqvist Å, Li H, Sommer L, Beatus P, Anderson DJ, Honjo T, et al. Notch signalling controls pancreatic cell differentiation. Nature. 1999 Aug;400(6747):877–81.
6. Apelqvist Å, Ahlgren U, Edlund H. Sonic hedgehog directs specialised mesoderm differentiation in the intestine and pancreas. Current Biology. 1997 Oct;7(10):801–4.
7. Krapp A, Knöfler M, Ledermann B, Bürki K, Berney C, Zoerkler N, et al. The bHLH protein PTF1-p48 is essential for the formation of the exocrine and the correct spatial organization of the endocrine pancreas. Genes Dev. 1998 Dec 1;12(23):3752–63.
8. Ahlgren U, Jonsson J, Edlund H. The morphogenesis of the pancreatic mesenchyme is uncoupled from that of the pancreatic epithelium in IPF1/PDX1-deficient mice. Development. 1996 May 1;122(5):1409–16.
9. Kawaguchi Y, Cooper B, Gannon M, Ray M, MacDonald RJ, Wright CVE. The role of the transcriptional regulator Ptf1a in converting intestinal to pancreatic progenitors. Nat Genet. 2002 Sep;32(1):128–34.
10. Mota-Reyes C, Gärtner P, Rosenkranz L, Grippo PJ, Ekin Demir I. In vivo Mouse Models of Pancreatic Ductal Adenocarcinoma. Pancreapedia: The Exocrine Pancreas Knowledge Base [Internet]. 2021 [cited 2023 May 9]; Available from: https://www.pancreapedia.org/node/9843
11. Feil R, Brocard J, Mascrez B, LeMeur M, Metzger D, Chambon P. Ligand-activated site-specific recombination in mice. Proceedings of the National Academy of Sciences. 1996 Oct;93(20):10887–90.
12. Desai BM, Oliver-Krasinski J, De Leon DD, Farzad C, Hong N, Leach SD, et al. Preexisting pancreatic acinar cells contribute to acinar cell, but not islet β cell, regeneration. Journal of Clinical Investigation. 2007 Apr 2;117(4):971–7.
13. Kopinke D, Brailsford M, Pan FC, Magnuson MA, Wright CVE, Murtaugh LC. Ongoing Notch signaling maintains phenotypic fidelity in the adult exocrine pancreas. Dev Biol [Internet]. 2012 Feb;362(1):57–64. Available from: https://linkinghub.elsevier.com/retrieve/pii/S0012160611013923

14. Habbe N, Shi G, Meguid RA, Fendrich V, Esni F, Chen H, et al. Spontaneous induction of murine pancreatic intraepithelial neoplasia (mPanIN) by acinar cell targeting of oncogenic Kras in adult mice. Proceedings of the National Academy of Sciences [Internet]. 2008 Dec 2;105(48):18913–8. Available from: https://pnas.org/doi/full/10.1073/pnas.0810097105
15. Jakubison BL, Schweickert PG, Moser SE, Yang Y, Gao H, Scully K, et al. Induced PTF1a expression in pancreatic ductal adenocarcinoma cells activates acinar gene networks, reduces tumorigenic properties, and sensitizes cells to gemcitabine treatment. Mol Oncol. 2018 Jun 1;12(7):1104–24.
16. Krah NM, De La O. JP, Swift GH, Hoang CQ, Willet SG, Pan FC, et al. The acinar differentiation determinant PTF1A inhibits initiation of pancreatic ductal adenocarcinoma. Elife. 2015 Jul 7;4(JULY2015).
17. Pin C, Fenech M. Development of the Pancreas. The Pancreapedia: Exocrine Pancreas Knowledge Base. 2017 Dec 12;
18. Pin CL, Rukstalis JM, Johnson C, Konieczny SF. The bHLH transcription factor Mist1 is required to maintain exocrine pancreas cell organization and acinar cell identity. Journal of Cell Biology. 2001 Nov 12;155(4):519–30.
19. Pin C. Mist1. The Pancreapedia: Exocrine Pancreas Knowledge Base. 2011 Jan 27;
20. Mills JC, Taghert PH. Scaling factors: Transcription factors regulating subcellular domains. BioEssays. 2012 Jan;34(1):10–6.
21. Direnzo D, Hess DA, Damsz B, Hallett JE, Marshall B, Goswami C, et al. Induced Mist1 Expression Promotes Remodeling of Mouse Pancreatic Acinar Cells. Gastroenterology. 2012 Aug;143(2):469–80.
22. Hess DA, Strelau KM, Karki A, Jiang M, Azevedo-Pouly AC, Lee AH, et al. MIST1 Links Secretion and Stress as both Target and Regulator of the Unfolded Protein Response. Mol Cell Biol. 2016 Dec 1;36(23):2931–44.
23. Shi G, DiRenzo D, Qu C, Barney D, Miley D, Konieczny SF. Maintenance of acinar cell organization is critical to preventing Kras-induced acinar-ductal metaplasia. Oncogene. 2013 Apr 11;32(15):1950–8.
24. Shi G, Zhu L, Sun Y, Bettencourt R, Damsz B, Hruban RH, et al. Loss of the Acinar-Restricted Transcription Factor Mist1 Accelerates Kras-Induced Pancreatic Intraepithelial Neoplasia. Gastroenterology. 2009 Apr;136(4):1368–78.
25. Sakikubo M, Furuyama K, Horiguchi M, Hosokawa S, Aoyama Y, Tsuboi K, et al. Ptf1a inactivation in adult pancreatic acinar cells causes apoptosis through activation of the endoplasmic reticulum stress pathway. Sci Rep. 2018 Oct 25;8(1):15812.
26. Johnson CL, Peat JM, Volante SN, Wang R, McLean CA, Pin CL. Activation of protein kinase Cδ leads to increased pancreatic acinar cell dedifferentiation in the absence of MIST1. J Pathol. 2012 Nov;228(3):351–65.
27. Azizi N, Toma J, Martin M, Khalid MF, Mousavi F, Win PW, et al. Loss of activating transcription factor 3 prevents KRAS-mediated pancreatic cancer. Oncogene. 2021 Apr 29;40(17):3118–35.
28. Ji B, Song J, Tsou L, Bi Y, Gaiser S, Mortensen R, et al. Robust acinar cell transgene expression of CreErT via BAC recombineering. Genesis. 2008 Aug;46(8):390–5.

29. Bankhead P, Loughrey MB, Fernández JA, Dombrowski Y, McArt DG, Dunne PD, et al. QuPath: Open source software for digital pathology image analysis. Sci Rep. 2017 Dec 4;7(1):16878.
30. Dobin A, Davis CA, Schlesinger F, Drenkow J, Zaleski C, Jha S, et al. STAR: ultrafast universal RNA-seq aligner. Bioinformatics. 2013 Jan 1;29(1):15–21.
31. Liao Y, Smyth GK, Shi W. featureCounts: an efficient general purpose program for assigning sequence reads to genomic features. Bioinformatics. 2014 Apr 1;30(7):923–30.
32. Love MI, Huber W, Anders S. Moderated estimation of fold change and dispersion for RNA-seq data with DESeq2. Genome Biol. 2014 Dec 5;15(12):550.
33. Yu G, Wang LG, Han Y, He QY. clusterProfiler: an R Package for Comparing Biological Themes Among Gene Clusters. OMICS. 2012 May;16(5):284–7.
34. Korotkevich G, Sukhov V, Budin N, Shpak B, Artyomov MN, Sergushichev A. Fast gene set enrichment analysis. bioRxiv [Internet]. 2021 Jan 1;060012. Available from: http://biorxiv.org/content/early/2021/02/01/060012.abstract
35. Kolde R. Pheatmap: pretty heatmaps. R package version. 2012;1(2):726.
36. Blighe Kevin, Aaron Lun. PCAtools: PCAtools: Everything Principal Components Analysis [Internet]. 2022 [cited 2023 May 18]. Available from: https://github.com/kevinblighe/PCAtools
37. Yu G. enrichplot: Visualization of Functional Enrichment Result [Internet]. 2023 [cited 2023 May 18]. Available from: https://yulab-smu.top/biomedical-knowledge-mining-book
38. Liberzon A, Birger C, Thorvaldsdóttir H, Ghandi M, Mesirov JP, Tamayo P. The Molecular Signatures Database Hallmark Gene Set Collection. Cell Syst. 2015 Dec;1(6):417–25.
39. Subramanian A, Tamayo P, Mootha VK, Mukherjee S, Ebert BL, Gillette MA, et al. Gene set enrichment analysis: A knowledge-based approach for interpreting genome-wide expression profiles. Proceedings of the National Academy of Sciences. 2005 Oct 25;102(43):15545–50.
40. Rouillard AD, Gundersen GW, Fernandez NF, Wang Z, Monteiro CD, McDermott MG, et al. The harmonizome: a collection of processed datasets gathered to serve and mine knowledge about genes and proteins. Database. 2016 Jul 3;2016:baw100.
41. Hingorani SR, Petricoin EF, Maitra A, Rajapakse V, King C, Jacobetz MA, et al. Preinvasive and invasive ductal pancreatic cancer and its early detection in the mouse. Cancer Cell [Internet]. 2003 Dec;4(6):437–50. Available from: https://linkinghub.elsevier.com/retrieve/pii/S153561080300309X
42. Krapp A, Knöfler M, Ledermann B, Bürki K, Berney C, Zoerkler N, et al. The bHLH protein PTF1-p48 is essential for the formation of the exocrine and the correct spatial organization of the endocrine pancreas. Genes Dev [Internet]. 1998 Dec 1;12(23):3752–63. Available from: http://genesdev.cshlp.org/lookup/doi/10.1101/gad.12.23.3752

43. Kawaguchi Y, Cooper B, Gannon M, Ray M, MacDonald RJ, Wright CVE. The role of the transcriptional regulator Ptf1a in converting intestinal to pancreatic progenitors. Nat Genet. 2002 Sep 19;32(1):128–34.
44. Pan FC, Bankaitis ED, Boyer D, Xu X, Van de Casteele M, Magnuson MA, et al. Spatiotemporal patterns of multipotentiality in *Ptf1a* -expressing cells during pancreas organogenesis and injury-induced facultative restoration. Development. 2013 Feb 15;140(4):751–64.
45. Krapp A, Knöfler M, Frutiger S, Hughes GJ, Hagenbüchle O, Wellauer PK. The p48 DNA-binding subunit of transcription factor PTF1 is a new exocrine pancreas-specific basic helix-loop-helix protein. EMBO J [Internet]. 1996 Aug 15;15(16):4317–29. Available from: http://www.ncbi.nlm.nih.gov/pubmed/8861960
46. Fukuda A, Kawaguchi Y, Furuyama K, Kodama S, Horiguchi M, Kuhara T, et al. Reduction of *Ptf1a* Gene Dosage Causes Pancreatic Hypoplasia and Diabetes in Mice. Diabetes. 2008 Sep 1;57(9):2421–31.
47. Dong PDS, Provost E, Leach SD, Stainier DYR. Graded levels of Ptf1a differentially regulate endocrine and exocrine fates in the developing pancreas. Genes Dev. 2008 Jun 1;22(11):1445–50.
48. Rodolosse A, Chalaux E, Adell T, Hagège H, Skoudy A, Real FX. PTF1α/p48 and cell proliferation. Gastroenterology. 2004 Sep;127(3):937–49.
49. Krah NM, Narayanan SM, Yugawa DE, Straley JA, Wright CVE, MacDonald RJ, et al. Prevention and Reversion of Pancreatic Tumorigenesis through a Differentiation-Based Mechanism. Dev Cell [Internet]. 2019 Sep;50(6):744-754.e4. Available from: https://linkinghub.elsevier.com/retrieve/pii/S1534580719305842
50. Hanahan D, Weinberg RA. Hallmarks of Cancer: The Next Generation. Cell. 2011 Mar;144(5):646–74.
51. Clark CE, Beatty GL, Vonderheide RH. Immunosurveillance of pancreatic adenocarcinoma: Insights from genetically engineered mouse models of cancer. Cancer Lett. 2009 Jun;279(1):1–7.
52. Zhang Y, Velez-Delgado A, Mathew E, Li D, Mendez FM, Flannagan K, et al. Myeloid cells are required for PD-1/PD-L1 checkpoint activation and the establishment of an immunosuppressive environment in pancreatic cancer. Gut. 2017 Jan;66(1):124–36.
53. Yang S, Liu Q, Liao Q. Tumor-Associated Macrophages in Pancreatic Ductal Adenocarcinoma: Origin, Polarization, Function, and Reprogramming. Front Cell Dev Biol. 2021 Jan 11;8.
54. Xu CR, Zaret KS. Chromatin “pre-pattern” and epigenetic modulation in the cell fate choice of liver over pancreas in the endoderm. Nucleus. 2012 Mar 27;3(2):150–4.
55. Stec N, Doerfel K, Hills-Muckey K, Ettorre VM, Ercan S, Keil W, et al. An Epigenetic Priming Mechanism Mediated by Nutrient Sensing Regulates Transcriptional Output during C. elegans Development. Current Biology. 2021 Feb;31(4):809-826.e6.

56. Flyamer IM, Gassler J, Imakaev M, Brandão HB, Ulianov S V., Abdennur N, et al. Single-nucleus Hi-C reveals unique chromatin reorganization at oocyte-to-zygote transition. Nature. 2017 Apr 29;544(7648):110–4.
57. Stec N, Doerfel K, Hills-Muckey K, Ettorre VM, Ercan S, Keil W, et al. An Epigenetic Priming Mechanism Mediated by Nutrient Sensing Regulates Transcriptional Output during C. elegans Development. Current Biology. 2021 Feb;31(4):809-826.e6.
58. Bernstein BE, Mikkelsen TS, Xie X, Kamal M, Huebert DJ, Cuff J, et al. A Bivalent Chromatin Structure Marks Key Developmental Genes in Embryonic Stem Cells. Cell. 2006 Apr;125(2):315–26.
59. Martínez-Cano J, Campos-Sánchez E, Cobaleda C. Epigenetic Priming in Immunodeficiencies. Front Cell Dev Biol. 2019 Jul 10;7.
60. Ernst C, Jefri M. Epigenetic priming in neurodevelopmental disorders. Trends Mol Med. 2021 Dec;27(12):1106–14.
61. Raboso-Gallego J, Casado-García A, Isidro-Hernández M, Vicente-Dueñas C. Epigenetic Priming in Childhood Acute Lymphoblastic Leukemia. Front Cell Dev Biol. 2019 Jul 17;7.
62. Mehmood R, Varga G, Mohanty SQ, Laing SW, Lu Y, Johnson CL, et al. Epigenetic Reprogramming in Mist1−/− Mice Predicts the Molecular Response to Cerulein-Induced Pancreatitis. Real FX, editor. PLoS One [Internet]. 2014 Jan 21;9(1):e84182. Available from: https://dx.plos.org/10.1371/journal.pone.0084182

Figure Legends:

Figure 1. KRAS^{G12D} activation promotes increased damage in a *Ptf1a* haploinsufficient background in response to pancreatic injury. (A) Schematic representation of creERT targeting to create inducible knock-in *Ptf1a*$^{creERT/+}$*KRAS*$^{G12D/+}$ (PK) and *Mist1*$^{creERT/+}$*KRAS*$^{G12D/+}$ (MK) mouse lines. **(B)** Representative H&E histology shows no difference between pancreatic morphology of *KRAS*$^{G12D/+}$ mice in *Ptf1a*$^{creERT/+}$ or *Mist1*$^{CreERT/+}$ cohorts 22 days following tamoxifen treatment. Magnification bar=100 µm. **(C)** Experimental timeline for tamoxifen and cerulein treatments. **(D)** H&E histology and **(E)** quantification of percent lesion area show more lesions formed in *Ptf1a*$^{creERT/+}$*KRAS*^{G12D} compared to *Mist1*$^{creERT/+}$*Kras*^{G12D} mice 5 weeks after cerulein treatment. Magnification bar= 500 µm. **(F)** IHC for amylase or CK19, and quantification of the percent **(G)** CK19 or **(H)** amylase positive area in *Ptf1a*$^{creERT/+}$*KRAS*^{G12D} and *Mist1*$^{creERT/+}$*KRAS*^{G12D} mice 5 weeks after cerulein treatment. Magnification bar= 200 µm. In all cases, $*p < 0.05$, $**p < 0.005$, $***p < 0.0005$. Significance was determined using a two-tailed unpaired t-test with Welch's correction. Error bars represent mean ± standard error. Each dot represents an individual mouse.

Figure 2. *Ptf1a*$^{creERT/+}$ mice show more damage than *Ela-creERT/KRAS*^{G12D} in response to KRAS^{G12D} activation following pancreatic injury. (A) Representative H&E histology of *Ela-creERT/KRAS*^{G12D} mice shows no lesions 22 days following tamoxifen treatment. **(B)** Timeline for tamoxifen and cerulein treatments of the *Ptf1a*$^{creERT/+}$*KRAS*$^{G12D/+}$ and *Ela-creERT/KRAS*^{G12D} mice. **(C)** Representative H&E

histology shows more lesions in *Ptf1a*$^{creERT/+}$*Kras*^{G12D} mice compared to *Ela-creERT/KRAS*^{G12D} mice 3 weeks after cerulein treatment. **(D)** IHC for amylase or CK19 and quantification of the % of tissue area positive for **(E)** CK19 or **(F)** amylase show increased CK19 and decreased amylase staining in *Ptf1a*$^{creERT/+}$*KRAS*^{G12D} mice compared to *Ela-creERT/KRAS*^{G12D} pancreata 3 weeks after cerulein treatment. $^{**}p < 0.01$, $^{****}p < 0.0001$. Significance was determined using a two-tailed unpaired t-test. Error bars represent mean ± standard error. Each dot represents an individual mouse. Magnification bars= 50 uM

Figure 3. The absence of one *Ptf1a* allele increases loss of the acinar cells in response to KRAS^{G12D} and injury. Timeline of tamoxifen (TX) and cerulein treatment for *Ptf1a*$^{creERT/+}$*KRAS*^{G12D} and **(A)** *Mist1*$^{creERT/+}$*KRAS*^{G12D} or **(C)** *Ela-creERT/KRAS*^{G12D} mice. Representative H&E histology shows more damage in the pancreas of *Ptf1a*$^{creERT/+}$*KRAS*^{G12D} than **(B)** *Mist1*$^{creERT/+}$*KRAS*^{G12D} or **(D)** *Ela-creERT/KRAS*^{G12D} mice 7 days after cerulein treatment. Magnification bar= 500 µm.

Figure 4. RNA-seq analysis reveals distinct gene expression profiles between *Ptf1a*$^{CreERT/+}$*Kras*^{G12D} and *Mist1*$^{CreERT/+}$*Kras*^{G12D} mice. (A, B) PCA plots showing clustering of *KRAS*^{G12D} and wild type (WT) RNA from pancreatic tissues of **(A)** *Ptf1a*$^{creERT/+}$*KRAS*^{G12D} (PK) and **(B)** *Mist1*$^{creERT/+}$*KRAS*^{G12D} (MK) mice. **(C, D)** Volcano plots comparing differentially-expressed genes (DEGs) between WT and **(C)** *Ptf1a*$^{creERT/+}$*KRAS*^{G12D} or **(D)** *Mist1*$^{creERT/+}$*KRAS*^{G12D} RNA-seq datasets. Number of differentially expressed genes are indicated on the graphs. In all cases, DEGs have p-

value < 0.05 and log_2FC> 1. **(E)** Gene Set Enrichment Analysis (GSEA) plot showing normalized enrichment score of the top Hallmark gene sets in *Ptf1a*$^{creERT/+}$*KRAS*^{G12D} and *Mist1*$^{creERT/+}$*KRAS*^{G12D} RNA compared to their corresponding wild type RNA samples.

Figure 5. KRAS signalling is enhanced by loss of a single *Ptf1a* allele. (A) GSEA plots for "Hallmark genes upregulated by KRAS activation" shows positive enrichment in *Ptf1a*$^{creERT/+}$*KRAS*^{G12D} but not *Mist1*$^{creERT/+}$*KRAS*^{G12D} RNA-seq datasets compared to their corresponding WT mice. **(B)** Bar plot for normalized read counts of *KRAS* expression based on *Ptf1a*$^{creERT/+}$*KRAS*^{G12D} (PK) and *Mist1*$^{creERT/+}$*KRAS*^{G12D} (MK) RNA-seq datasets show no difference in *KRAS* expression compared to wild type (WT). Significance was determined using a two-tailed unpaired t-test with Welch's correction. Error bars represent mean ± standard error. N values are indicated on top of each bar. **(C)** Heatmap for Log_2 of normalized read counts of genes in the KEGG pathway for MAPK Signaling shows increased expression of these genes in the *Ptf1a*$^{creERT/+}$*KRAS*^{G12D} mice compared to WT. **(D)** IHC for FOS (upper panels) and JUN (lower panels) shows more positive nuclei in *Ptf1a*$^{CreERT/+}$*Kras*^{G12D} tissue compared to *Mist1*$^{creERT/+}$*KRAS*^{G12D} tissue for FPS but not JUN. Magnification bar= 500 µm. **(E)** RNA tracks showing expression level of Fos (left) and Jun (right) in the *Mist1*$^{creERT/+}$*KRAS*^{G12D} tissue and its corresponding wild type and the *Ptf1a*$^{creERT/+}$*KRAS*^{G12D} tissue and its corresponding wild type tissue.

Figure 6. A distinct inflammatory response is activated in the *Ptf1a*$^{CreERT/+}$*Kras*^{G12D} model. (A) Dotplot and **(B)** Cnet plot shows top Gene Ontology (GO) pathways enriched in *Ptf1a*$^{creERT/+}$*KRAS*^{G12D} (PK) and *Mist1*$^{creERT/+}$*KRAS*^{G12D} (MK) tissue. Immune-related terms are over-represented in the *Ptf1a*$^{creERT/+}$*KRAS*^{G12D} dataset but not in *Mist1*$^{creERT/+}$*KRAS*^{G12D}. The analysis was performed using DEGs with a p-value <0.05 and $\log_2$FC> 1. **(C)** GSEA plots for Hallmark "Genes in the Inflammatory Response" in the MSigDB database shows positive enrichment scores for *Ptf1a*$^{creERT/+}$*KRAS*^{G12D} but not *Mist1*$^{creERT/+}$*KRAS*^{G12D} compared to the corresponding wild type cohorts.

Figure 7. Macrophage and CD3+ T-cell infiltration is increased in the *Ptf1a*$^{creERT/+}$*KRAS*^{G12D} pancreas. (A) Opal Multiplex assays for CK19 and multiple immune marks, including F4/80 (macrophage marker), CD8+ (cytotoxic) T-cells, and CD3^{+} T-cells show increased CK19, F4/80 and CD3+ accumulations in the *Ptf1a*$^{creERT/+}$*KRAS*^{G12D} (PK) pancreas compared to *Mist1*$^{creERT/+}$*KRAS*^{G12D} (MK) tissue. **(B-E)** Scatter plots displaying the percent of CK19+, F4/80+, CD8+, and CD3+ cells per tile in *Ptf1a*$^{creERT/+}$*KRAS*^{G12D}, *Mist1*$^{creERT/+}$*KRAS*^{G12D}, and wild type (WT) pancreata. In all cases, $^{**}p < 0.005$, $^{***}p < 0.0005$, and $^{****}p < 0.0001$. Significance was determined using Kruskal-Wallis rank sum test and subsequent pairwise Wilcoxon rank sum test . Error bars represent mean ± standard error. **(F)** Heatmap showing expression level and clustering of each immune marker in the wild type (Ctrl), *Ptf1a*$^{CreERT/+}$*Kras*^{G12D} and *Mist1*$^{CreERT/+}$*Kras*^{G12D} tissue, following quantification on the QuPath software. **G)** Scatter plot visualizing percentage of cells stained with F4/80 against those stained with CK19 in WT, *Ptf1a*$^{creERT/+}$*KRAS*^{G12D}, and *Mist1*$^{creERT/+}$*KRAS*^{G12D} tissue.

Figure 8. Macrophage and CD3+ T-cell infiltration is increased in the *Ptf1a*$^{creERT/+}$*KRAS*^{G12D} pancreas. (A) Opal Multiplex assays for CK19 and multiple immune marks, including F4/80 (macrophage marker), CD8+ (cytotoxic) T-cells, and CD3^{+} T-cells show increased CK19, F4/80 and CD3+ accumulations in the *Ptf1a*$^{creERT/+}$*KRAS*^{G12D} (PK) pancreas compared to *Ela-creERT/KRAS*^{G12D} (EK) tissue. **(B-E)** Scatter plots displaying the percent of CK19+, F4/80+, CD8+, and CD3+ cells per tile in *Ptf1a*$^{creERT/+}$*KRAS*^{G12D}, *Ela-creERT/KRAS*^{G12D}, and wild type (WT) pancreata. In all cases, $*p < 0.05$, $**p < 0.005$, $***p < 0.0005$, and $****p < 0.0001$. Significance was determined using Kruskal-Wallis rank sum test and subsequent pairwise Wilcoxon rank sum test. Error bars represent mean ± standard error. **(F)** Heatmap showing expression level and clustering of each immune marker in the wild type (Ctrl), *Ptf1a*$^{CreERT/+}$*Kras*^{G12D} and *Ela-creERT/KRAS*^{G12D} tissue, following quantification on the QuPath software. **G)** Scatter plot visualizing percentage of cells stained with F4/80 against those stained with CK19 in WT, *Ptf1a*$^{creERT/+}$*KRAS*^{G12D}, and *Ela-creERT/KRAS*^{G12D} tissue.

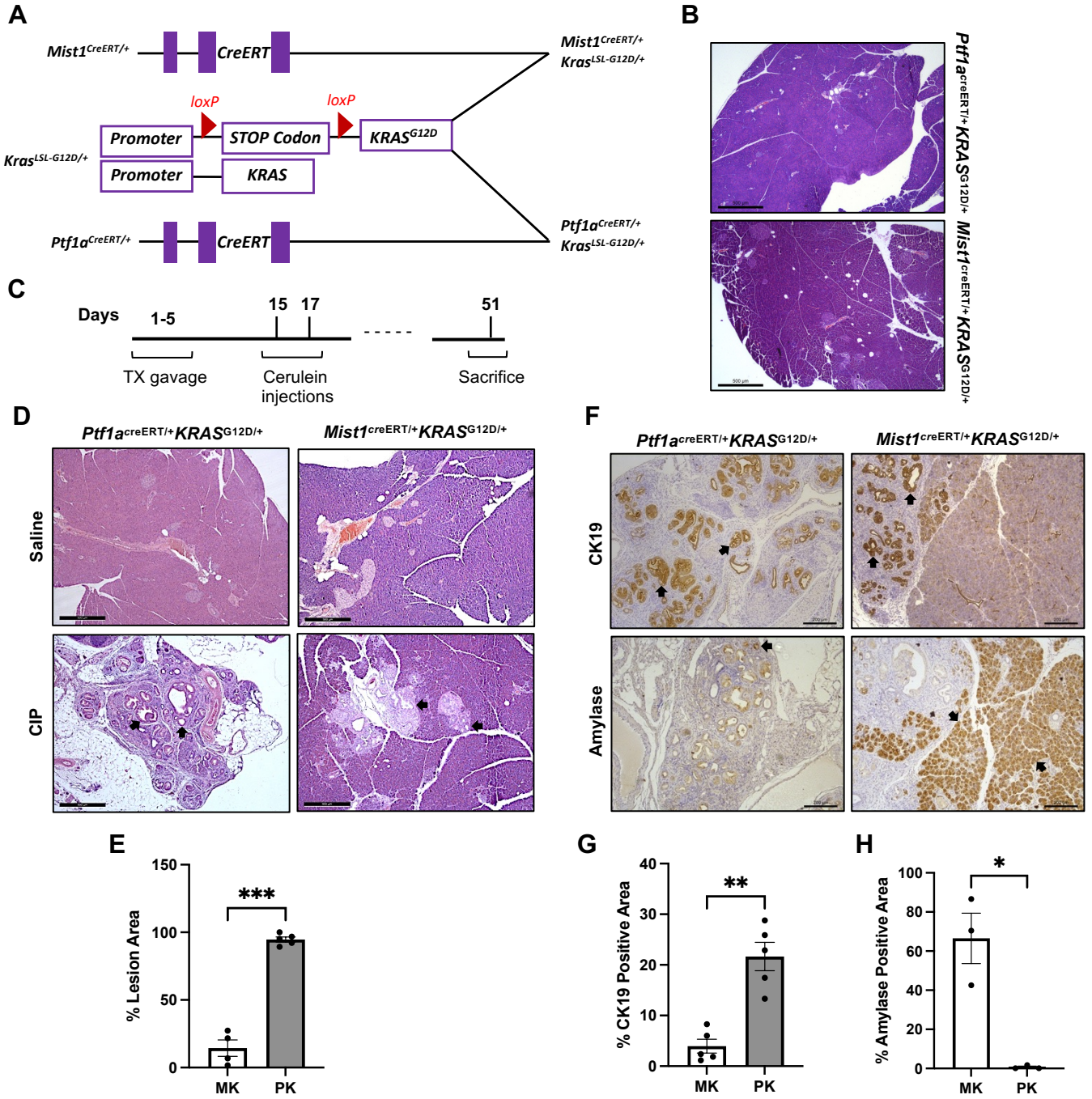

Mousavi et al (2023) Figure 1. KRAS^{G12D} activation promotes increased damage in a *Ptf1a* haploinsufficient background in response to pancreatic injury. (A) Schematic representation of creERT targeting to create inducible knock-in *Ptf1a*$^{creERT/+}$*KRAS*$^{G12D/+}$ (PK) and *Mist1*$^{creERT/+}$*KRAS*$^{G12D/+}$ (MK) mouse lines. **(B)** Representative H&E histology shows no difference between pancreatic morphology of *KRAS*$^{G12D/+}$ mice in *Ptf1a*$^{creERT/+}$ or *Mist1*$^{CreERT/+}$ cohorts 22 days following tamoxifen treatment. Magnification bar=100 µm. **(C)** Experimental timeline for tamoxifen and cerulein treatments. **(D)** H&E histology and **(E)** quantification of percent lesion area show more lesions formed in *Ptf1a*$^{creERT/+}$*KRAS*^{G12D} compared to *Mist1*$^{creERT/+}$*Kras*^{G12D} mice 5 weeks after cerulein treatment. Magnification bar= 500 µm. **(F)** IHC for amylase or CK19, and quantification of the percent **(G)** CK19 or **(H)** amylase positive area in *Ptf1a*$^{creERT/+}$*KRAS*^{G12D} and *Mist1*$^{creERT/+}$*KRAS*^{G12D} mice 5 weeks after cerulein treatment. Magnification bar= 200 µm. In all cases, $^{*}p < 0.05$, $^{**}p < 0.005$, $^{***}p < 0.0005$. Significance was determined using a two-tailed unpaired t-test with Welch's correction. Error bars represent mean ± standard error. Each dot represents an individual mouse.

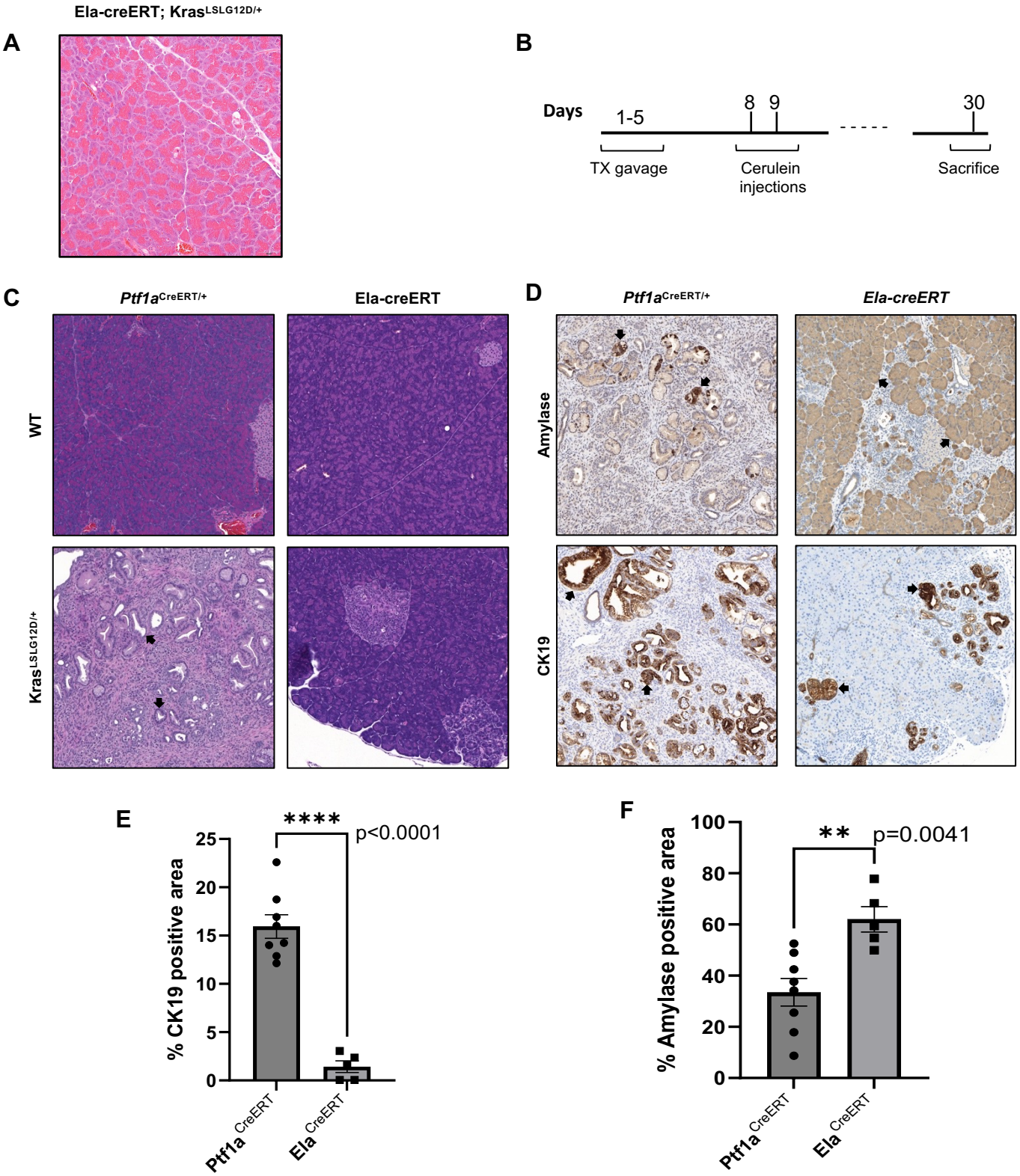

Mousavi et al (2023) Figure 2. *Ptf1a*$^{creERT/+}$ mice show more damage than *Ela-creERT/KRAS*^{G12D} in response to KRAS^{G12D} activation following pancreatic injury. (A) Representative H&E histology of *Ela-creERT/KRAS*^{G12D} mice shows no lesions 22 days following tamoxifen treatment. **(B)** Timeline for tamoxifen and cerulein treatments of the *Ptf1a*$^{creERT/+}$*KRAS*$^{G12D/+}$ and *Ela-creERT/KRAS*^{G12D} mice. **(C)** Representative H&E histology shows more lesions in *Ptf1a*$^{creERT/+}$*Kras*^{G12D} mice compared to *Ela-creERT/KRAS*^{G12D} mice 3 weeks after cerulein treatment. **(D)** IHC for amylase or CK19 and quantification of the % of tissue area positive for **(E)** CK19 or **(F)** amylase show increased CK19 and decreased amylase staining in *Ptf1a*$^{creERT/+}$*KRAS*^{G12D} mice compared to *Ela-creERT/KRAS*^{G12D} pancreata 3 weeks after cerulein treatment. $^{**}p < 0.01$, $^{****}p < 0.0001$. Significance was determined using a two-tailed unpaired t-test. Error bars represent mean ± standard error. Each dot represents an individual mouse. Magnification bars= 50 uM

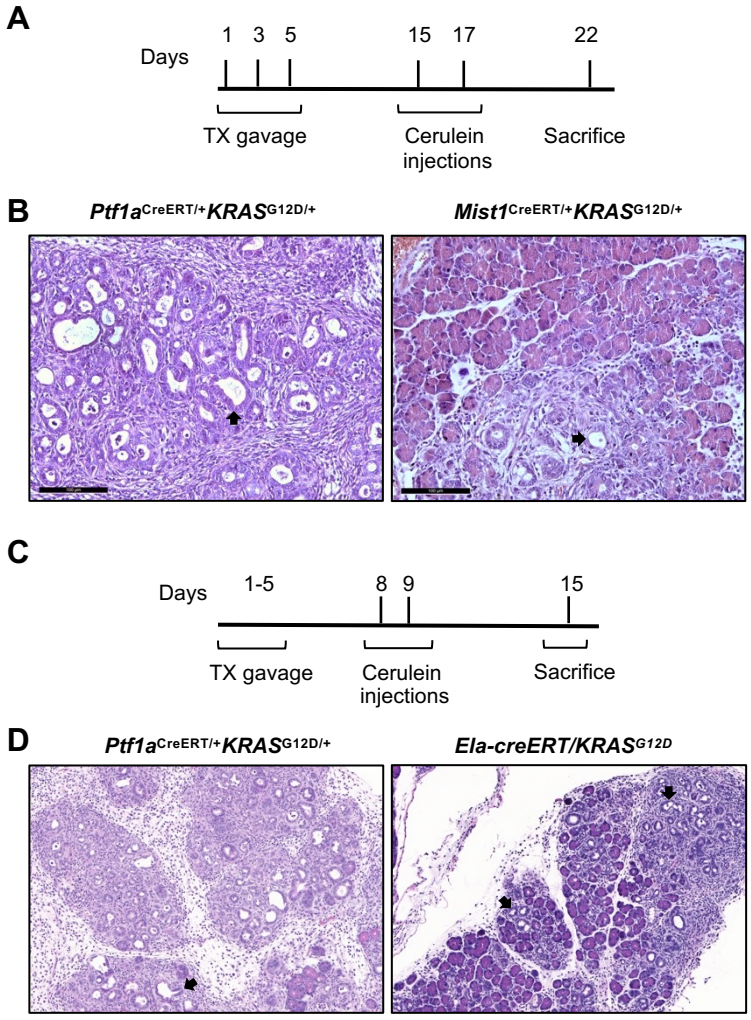

Mousavi et al (2023) Figure 3. The absence of one *Ptf1a* allele increases loss of the acinar cells in response to KRAS^{G12D} and injury. Timeline of tamoxifen (TX) and cerulein treatment for *Ptf1a$^{creERT/+}$KRAS^{G12D}* and **(A)** *Mist1$^{creERT/+}$KRAS^{G12D}* or **(C)** *Ela-creERT/KRAS^{G12D}* mice. Representative H&E histology shows more damage in the pancreas of *Ptf1a$^{creERT/+}$KRAS^{G12D}* than **(B)** *Mist1$^{creERT/+}$KRAS^{G12D}* or **(D)** *Ela-creERT/KRAS^{G12D}* mice 7 days after cerulein treatment. Magnification bar= 500 µm.

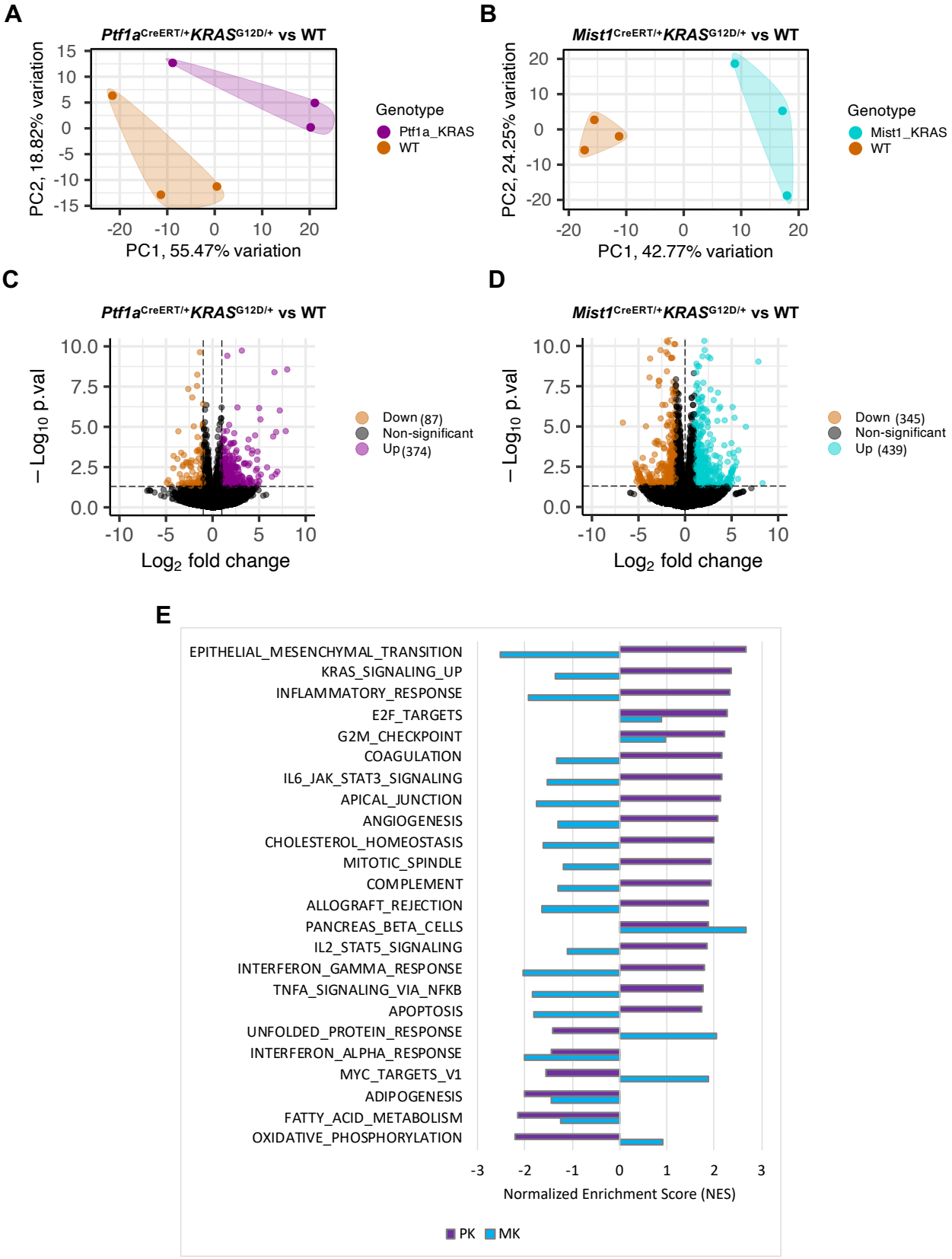

Mousavi et al (2023) Figure 4. RNA-seq analysis reveals distinct gene expression profiles between *Ptf1a*$^{CreERT/+}$*Kras*^{G12D} and *Mist1*$^{CreERT/+}$*Kras*^{G12D} mice. (A, B) PCA plots showing clustering of *KRAS*^{G12D} and wild type (WT) RNA from pancreatic tissues of **(A)** *Ptf1a*$^{creERT/+}$*KRAS*^{G12D} (PK) and **(B)** *Mist1*$^{creERT/+}$*KRAS*^{G12D} (MK) mice. **(C, D)** Volcano plots comparing differentially-expressed genes (DEGs) between WT and **(C)** *Ptf1a*$^{creERT/+}$*KRAS*^{G12D} or **(D)** *Mist1*$^{creERT/+}$*KRAS*^{G12D} RNA-seq datasets. Number of differentially expressed genes are indicated on the graphs. In all cases, DEGs have p-value < 0.05 and $\log_2$FC> 1. **(E)** Gene Set Enrichment Analysis (GSEA) plot showing normalized enrichment score of the top Hallmark gene sets in *Ptf1a*$^{creERT/+}$*KRAS*^{G12D} and *Mist1*$^{creERT/+}$*KRAS*^{G12D} RNA compared to their corresponding WT RNA samples.

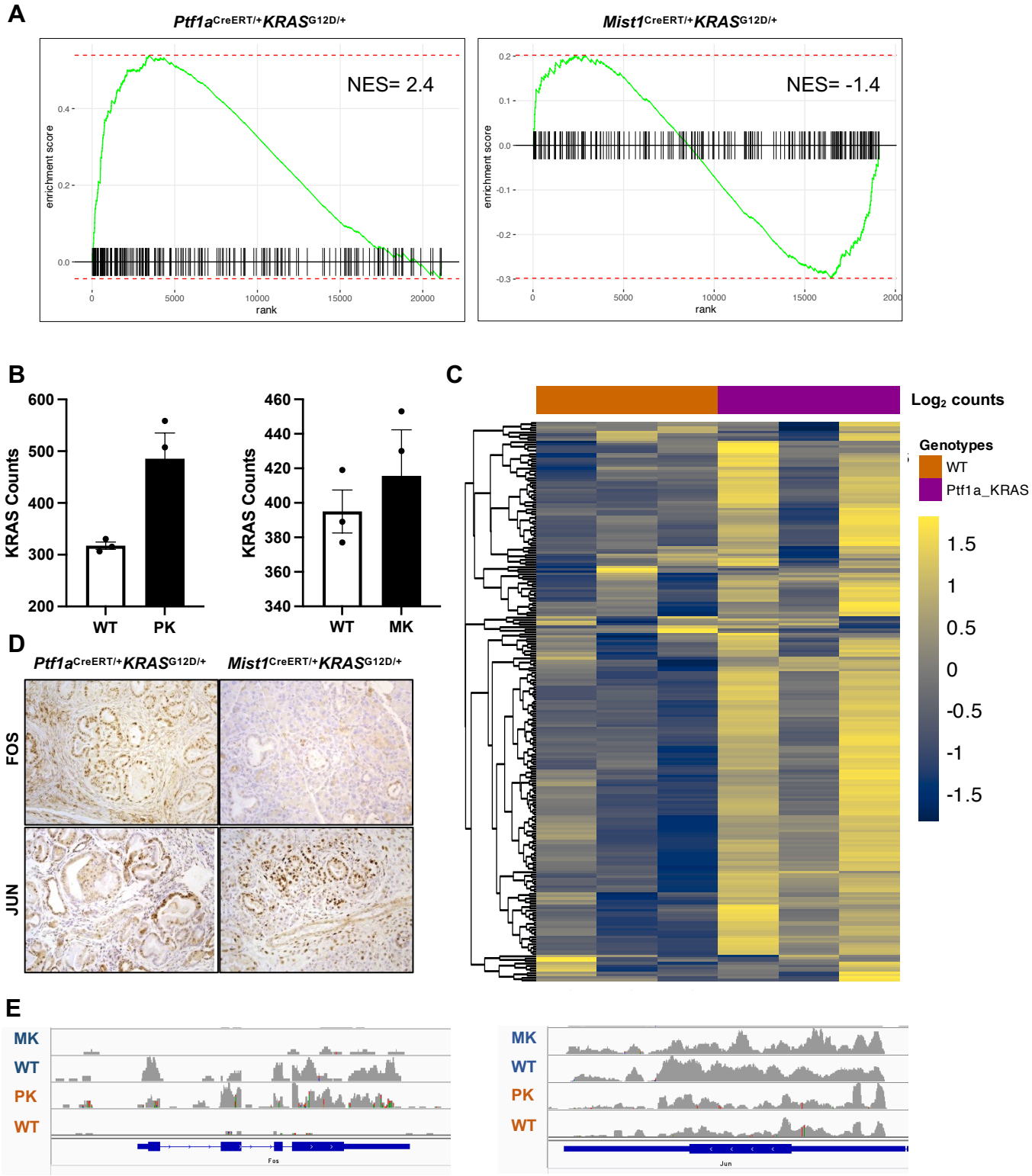

Mousavi et al (2023) Figure 5. KRAS signalling is enhanced by loss of a single *Ptf1a* allele. (A) GSEA plots for "Hallmark genes upregulated by KRAS activation" shows positive enrichment in *Ptf1a*$^{creERT/+}$*KRAS*^{G12D} but not *Mist1*$^{creERT/+}$*KRAS*^{G12D} RNA-seq datasets compared to their corresponding WT mice. **(B)** Bar plot for normalized read counts of *KRAS* expression based on *Ptf1a*$^{creERT/+}$*KRAS*^{G12D} (PK) and *Mist1*$^{creERT/+}$*KRAS*^{G12D} (MK) RNA-seq datasets show no difference in *KRAS* expression compared to wild type (WT). Significance was determined using a two-tailed unpaired t-test with Welch's correction. Error bars represent mean ± standard error. N values are indicated on top of each bar. **(C)** Heatmap for Log_2 of normalized read counts of genes in the KEGG pathway for MAPK Signaling shows increased expression of these genes in the *Ptf1a*$^{creERT/+}$*KRAS*^{G12D} mice compared to WT. **(D)** IHC for FOS (upper panels) and JUN (lower panels) shows more positive nuclei in *Ptf1a*$^{CreERT/+}$*Kras*^{G12D} tissue compared to *Mist1*$^{creERT/+}$*KRAS*^{G12D} tissue for FPS but not JUN. Magnification bar= 500 µm. **(E)** RNA tracks showing expression level of Fos (left) and Jun (right) in the *Mist1*$^{creERT/+}$*KRAS*^{G12D} tissue and its corresponding wild type and the *Ptf1a*$^{creERT/+}$*KRAS*^{G12D} tissue and its corresponding wild type tissue.

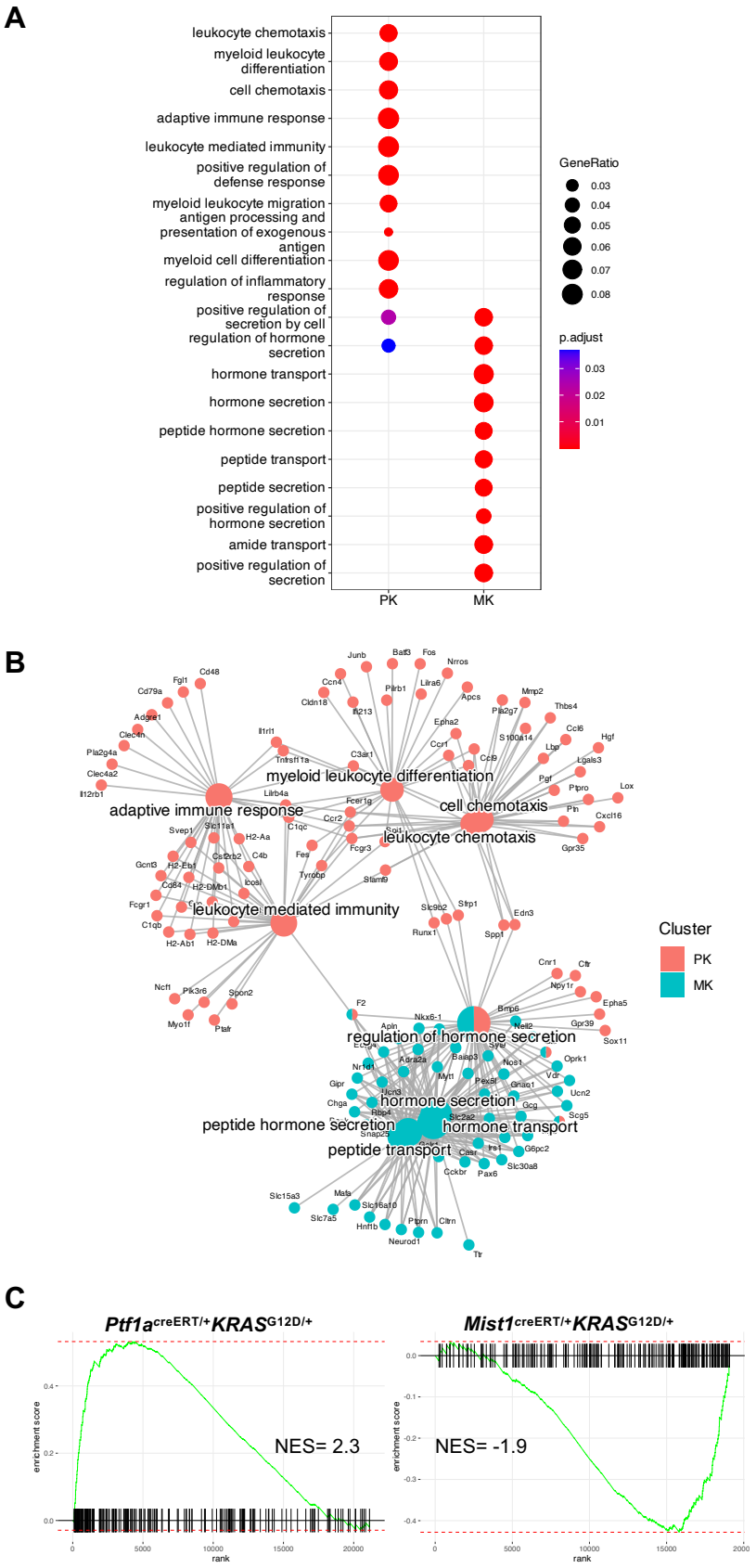

Mousavi et al (2023) Figure 6. A distinct inflammatory response is activated in the *Ptf1a*$^{CreERT/+}$*Kras*^{G12D} model. (A) Dotplot and **(B)** Cnet plot shows top Gene Ontology (GO) pathways enriched in *Ptf1a*$^{creERT/+}$*KRAS*^{G12D} (PK) and *Mist1*$^{creERT/+}$*KRAS*^{G12D} (MK) tissue. Immune-related terms are over-represented in the *Ptf1a*$^{creERT/+}$*KRAS*^{G12D} dataset but not in *Mist1*$^{creERT/+}$*KRAS*^{G12D}. The analysis was performed using DEGs with a p-value <0.05 and $\log_2$FC> 1. **(C)** GSEA plots for Hallmark "Genes in the Inflammatory Response" in the MSigDB database shows positive enrichment scores for *Ptf1a*$^{creERT/+}$*KRAS*^{G12D} but not *Mist1*$^{creERT/+}$*KRAS*^{G12D} compared to the corresponding wild type cohorts.

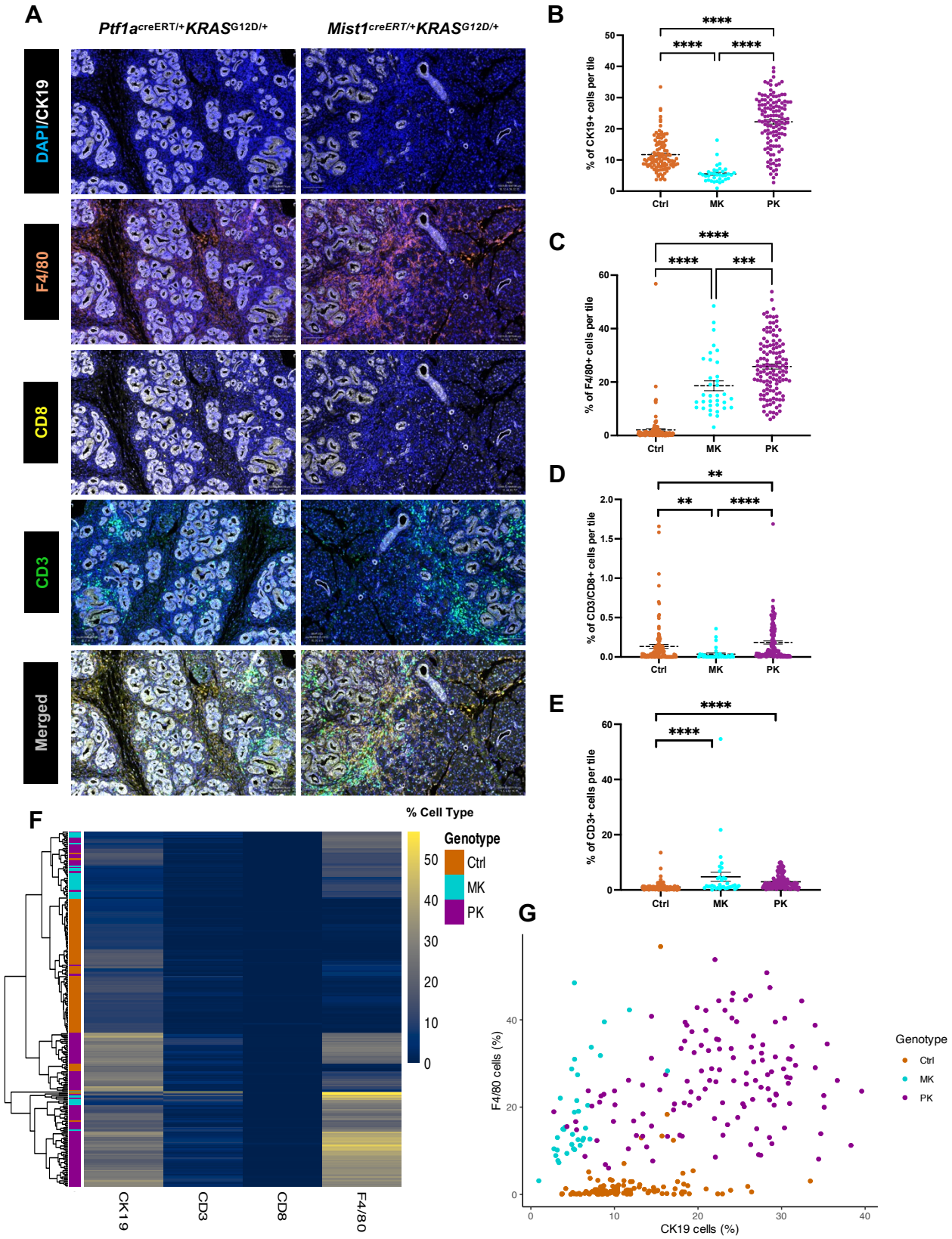

Mousavi et al (2023) Figure 7. Macrophage and CD3+ T-cell infiltration is increased in the *Ptf1a*$^{creERT/+}$*KRAS*^{G12D} pancreas. (A) Opal Multiplex assays for CK19 and multiple immune marks, including F4/80 (macrophage marker), CD8+ (cytotoxic) T-cells, and CD3^{+} T-cells show increased CK19, F4/80 and CD3+ accumulations in the *Ptf1a*$^{creERT/+}$*KRAS*^{G12D} (PK) pancreas compared to *Mist1*$^{creERT/+}$*KRAS*^{G12D} (MK) tissue. **(B-E)** Scatter plots displaying the percent of CK19+, F4/80+, CD8+, and CD3+ cells per tile in *Ptf1a*$^{creERT/+}$*KRAS*^{G12D}, *Mist1*$^{creERT/+}$*KRAS*^{G12D}, and wild type (WT) pancreata. In all cases, $^{**}p < 0.005$, $^{***}p < 0.0005$, and $^{****}p < 0.0001$. Significance was determined using Kruskal-Wallis rank sum test and subsequent pairwise Wilcoxon rank sum test . Error bars represent mean ± standard error. **(F)** Heatmap showing expression level and clustering of each immune marker in the wild type (Ctrl), *Ptf1a*$^{CreERT/+}$*Kras*^{G12D} and *Mist1*$^{CreERT/+}$*Kras*^{G12D} tissue, following quantification on the QuPath software. **G)** Scatter plot visualizing percentage of cells stained with F4/80 against those stained with CK19 in WT, *Ptf1a*$^{creERT/+}$*KRAS*^{G12D}, and *Mist1*$^{creERT/+}$*KRAS*^{G12D} tissue.

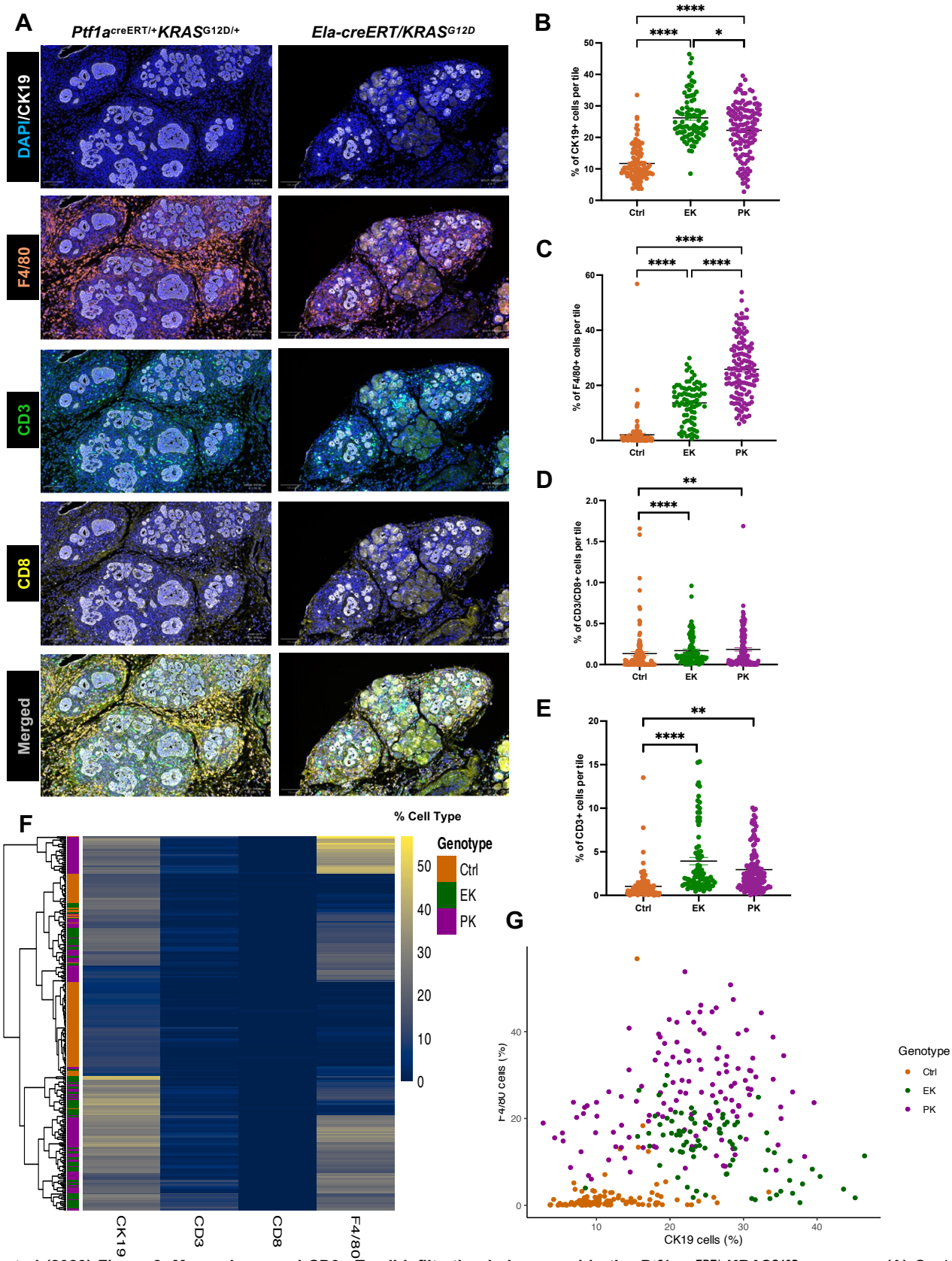

Mousavi et al (2023) Figure 8. Macrophage and CD3+ T-cell infiltration is increased in the *Ptf1a*$^{creERT/+}$*KRAS*^{G12D} pancreas. (A) Opal Multiplex assays for CK19 and multiple immune marks, including F4/80 (macrophage marker), CD8+ (cytotoxic) T-cells, and CD3^{+} T-cells show increased CK19, F4/80 and CD3+ accumulations in the *Ptf1a*$^{creERT/+}$*KRAS*^{G12D} (PK) pancreas compared to *Ela-creERT/KRAS*^{G12D} (EK) tissue. **(B-E)** Scatter plots displaying the percent of CK19+, F4/80+, CD8+, and CD3+ cells per tile in *Ptf1a*$^{creERT/+}$*KRAS*^{G12D}, *Ela-creERT/KRAS*^{G12D}, and wild type (WT) pancreata. In all cases, $*p < 0.05$, $**p < 0.005$, $***p < 0.0005$, and $****p < 0.0001$. Significance was determined using Kruskal-Wallis rank sum test and subsequent pairwise Wilcoxon rank sum test. Error bars represent mean ± standard error. **(F)** Heatmap showing expression level and clustering of each immune marker in the wild type (Ctrl), *Ptf1a*$^{CreERT/+}$*Kras*^{G12D} and *Ela-creERT/KRAS*^{G12D} tissue, following quantification on the QuPath software. **G)** Scatter plot visualizing percentage of cells stained with F4/80 against those stained with CK19 in WT, *Ptf1a*$^{creERT/+}$*KRAS*^{G12D}, and *Ela-creERT/KRAS*^{G12D} tissue.